



HAL
open science

The Chiral Dipolar Hard Sphere Model.

Martial Mazars

► **To cite this version:**

Martial Mazars. The Chiral Dipolar Hard Sphere Model.. Molecular Physics, 2009, 107 (04-06), pp.467-486. <10.1080/00268970902852640>. <hal-00513273>

HAL Id: hal-00513273

<https://hal.science/hal-00513273v1>

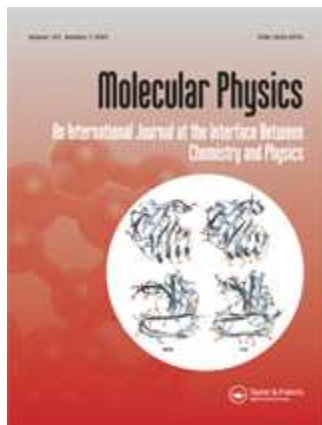
Submitted on 1 Sep 2010

HAL is a multi-disciplinary open access archive for the deposit and dissemination of scientific research documents, whether they are published or not. The documents may come from teaching and research institutions in France or abroad, or from public or private research centers.

L'archive ouverte pluridisciplinaire HAL, est destinée au dépôt et à la diffusion de documents scientifiques de niveau recherche, publiés ou non, émanant des établissements d'enseignement et de recherche français ou étrangers, des laboratoires publics ou privés.



HAL Authorization



The Chiral Dipolar Hard Sphere Model.

Journal:	<i>Molecular Physics</i>
Manuscript ID:	TMPH-2009-0027.R1
Manuscript Type:	Special Issue Paper - Dr. Jean-Jacques Weis
Date Submitted by the Author:	19-Feb-2009
Complete List of Authors:	Mazars, Martial; Université de Paris Sud XI, Laboratoire de Physique Théorique
Keywords:	Chirality, Monte-Carlo simulations, Liquid Crystals
Note: The following files were submitted by the author for peer review, but cannot be converted to PDF. You must view these files (e.g. movies) online.	
Mazars_TMPH_2009_0027.tex	



RESEARCH ARTICLE

The Chiral Dipolar Hard Sphere Model.

Martial Mazars *

Laboratoire de Physique Théorique (UMR 8627), Université de Paris Sud XI, Bâtiment
210, 91405 Orsay Cedex, FRANCE.

()

A simple molecular model of chiral molecules is presented in this paper : the chiral dipolar hard sphere model. The discriminatory interaction between enantiomers is represented by electrostatic (or magnetic) dipoles-dipoles interactions : short ranged steric repulsion are represented by hard sphere potential and, in each molecule, two point dipoles are located inside the sphere. The model is described in detail and some of its elementary properties are given ; in particular, it is shown that the knowledge of only three multipole spherical components (namely : Q_{10} , Q_{21} and Q_{22}) allows to compute all multipole spherical components of the model. Despite the simplicity of the model, it is shown also that the energy landscape of the interaction between two enantiomers is quite rich, this renders systems of chiral dipolar hard sphere very interesting and complicated to study. Few preliminary Monte Carlo simulation results are also reported in the paper. Last, but not least, this paper is dedicated to Jean-Jacques Weis.

1. Introduction

Chirality is used to describe a lack of symmetry in compounds : it refers to objects, molecules or structures that are not superposable on their mirror image. The separation of the two optical active forms of the tartaric acid, based on the observation of the symmetry of crystals by Pasteur in 1847, has been a major step in the understanding of optical properties of crystals and liquids [1]. Later, in 1884, Kelvin introduced the term chirality, but it has been extensively and systematically used only eighty years later with the introduction of the Cahn-Ingold-Prelog priority rules [2]. Since Arago, Biot and Pasteur, the ideas and concepts on optical activity of substances and on chirality have had and still have a lot of applications in chemistry, biology and physics.

In chemistry and biochemistry, chirality is an important tool in stereochemistry and for the determination of the functions of molecules. The interactions between biological molecules are frequently a consequence of the chiral interactions between them. For instance, as first noted by Pasteur, the two forms of asparagine (*dextro* and *levo*) tasted differently ; it was found later that this is a frequent property the two optical active forms of amino acids, because of the chiral structure of the taste bud receptor site (several others interesting examples may be found in [3]). The helical structures of DNA, RNA, proteins, etc. are also important to permit biological recognition and interactions between biological structures [4, 5].

In condensed matter physics many properties depend on the chirality of constituents or structures. More specifically, in liquid crystal physics, many phases as cholesteric, some smectics phases (S_A^* , S_C^* , etc.) and blue phases possess an optical

*Corresponding author. Email: Martial.Mazars@th.u-psud.fr

1 rotatory power [6–12] ; in most cases, a helical arrangement of the molecules is re-
2 sponsible for this property. Obviously, these properties are of a particular interest
3 for technological applications. It is not necessary for the molecules to be chiral to
4 observe chiral liquid crystal phases [10, 13, 14] ; however, some particular phases,
5 such as the ferroelectric smectic- C^* phase, may be observed only when some chiral
6 molecules are present in the sample (see section 5.10 of ref.[9] and refs.[15–17]).

7 To describe the optical activity of liquids and solids, and the discriminatory inter-
8 action between chiral molecules several molecular models have been built. Among
9 the most known are Kuhn models that are based on coupled-oscillators arranged
10 on an asymmetric tetrahedron [18, 19], the optical activity tensor or gyration po-
11 larizability may be computed in these models [20–22]. Models based on chirality of
12 helix have also been used [21, 23, 24]. These helical models are important for the
13 study of the properties of carbon nanotubes [25–27] and biological macromolecules
14 [4, 28, 29].

15 For the study of chirality in fluids and solids, the discriminatory interactions be-
16 tween enantiomers are important too [3]. The difference in the interaction between
17 enantiomeric molecules may have several origins, it may stems from steric, electro-
18 static, magnetic or dispersion interactions [3, 31, 32]. These *chirodiastaltic* interac-
19 tions [30] are responsible for some differences in thermodynamical and structural
20 properties between enantiopure systems (homochiral systems - systems that are
21 composed with exclusively one enantiomer) and racemic systems (systems com-
22 posed in equal proportions of the two enantiomers). For instance, the melting
23 point of crystals of the enantiomeric pure (+)-tartaric acid is 170°C , while, for
24 the racemic crystals, the melting temperature is $204 - 6^\circ\text{C}$. Some differences are
25 also reported for boiling points, but since the chirodiastaltic interactions are quite
26 small in general, these difference in boiling points are small and do not occur sys-
27 tematically. In liquid crystals, the phase diagrams depend also on the fractional
28 concentrations of enantiomers [33].

29 Several simple molecular models have been proposed and used to study the ther-
30 modynamical and structural properties of fluids and solids of chiral molecules in
31 computer simulations and integral equation theories. In these simple molecular
32 models, the chirodiastaltic interactions are represented either via steric interac-
33 tions [34–38] or electrostatic interactions [39–42] ; a chiral Gay-Berne model has
34 also been built [43]. In the present work, we describe another simple model of chiral
35 molecules, the chiral dipolar hard sphere model. In this model, the chirodiastaltic
36 interactions is represented by electrostatic (or magnetic) dipoles-dipoles interac-
37 tions, it consists of hard sphere with two point dipoles located inside the molecule.
38 As shown by Craig and coworkers, electrostatic interactions between enantiomers
39 may be discriminatory at most if the dipole-quadrupole interaction between two
40 enantiomers differs [3, 44, 45] ; this implies that if the quadrupole moment of the
41 two form of enantiomers differs then the interaction may be discriminatory. There-
42 fore, a chiral model based on electrostatic interactions must have at least four point
43 electric charges arranged on an asymmetric tetrahedron geometry, as the models in
44 refs.[39–42], two non-colinear point dipoles [46] or one quadrupole with no planar
45 symmetry [44].

46 The present paper is organised as follow. In section 2, we describe the model of
47 chiral dipolar hard sphere in detail and give some of its elementary properties.
48 More precisely, in section 2.1, we define the model, the nomenclature, its pertinent
49 parameters and we compute all its multipole moments ; it is shown that the knowl-
50 edge of only three multipole spherical components (namely : Q_{10} , Q_{21} and Q_{22})
51 allows to compute all multipole spherical components of the model. **The knowledge
52 of all multipole moments is important in the definition of the model and in the**

determination of its electrical properties and also, in view of the determination of the optical activity of the model, for the computation of multipole-multipole polarizabilities [3, 19, 44, 45, 47–50]. In section 2.2, we compute interaction energies between two enantiomers in some particular configurations ; it is shown that, despite the simplicity of the molecular model, the energy landscape of the interaction between two enantiomers is quite complicated. In section 3, we report some preliminary results of Monte Carlo simulations performed in the canonical (NVT) and isobaric (NPT) ensembles ; in these computations, all dipole-dipole interactions between molecules are explicitly taken into account by using the Ewald method for dipolar interactions [51]. The paper ends with a discussion on the perspectives that this model offers to the study of chiral fluids and solids. For completeness, in appendix A, we give general formulas for the computation of multipole moments for any dipole distribution.

Last, but not least, this paper is dedicated to my colleague Jean-Jacques Weis.

2. Elementary properties of chiral dipolar hard sphere model.

In this section, we describe the chiral dipolar hard sphere model and we give some of its elementary properties. The subsection 2.1 is devoted to the definition of the model and to the computation of the multipole moments due to the two permanent dipoles moments ; all multipole moments are computed with the center of the sphere taken as origin.

In subsection 2.2, we compute interaction energies between two enantiomers for few particular configurations ; in this subsection, a particular attention is pay to the *chirodiastaltic* interactions for colinear aligned total dipole moments and antiparallel dipole moment configurations. The discriminatory interaction energies are often computed by using the multipole expansion [3, 22, 24, 39, 41, 44, 47, 49, 50] ; thus, to facilitate the comparison with these works, the discriminatory interaction energies between chiral dipolar hard sphere have also been computed analytically by using the multipole expansion when the distance between both enantiomers is large in comparison to their diameter. However, if both enantiomers are at contact or if the distance between them is too small to use with accuracy the multipole expansion, then the interaction energies must be computed by summing all dipole-dipole interactions ; it is done so in subsection 2.2 for all configurations at contact and in section in all Monte-Carlo computations done with the Ewald method.

2.1. Definition of the model and its multipole moments.

The Chiral Dipolar Hard Sphere model consist of hard spheres of diameter σ with two point dipoles $\boldsymbol{\mu}_1$ and $\boldsymbol{\mu}_2$ located at points O_1 and O_2 inside the sphere. We define the molecular axis $\hat{\boldsymbol{u}}$ of a chiral dipolar hard sphere as $\boldsymbol{O}_1\boldsymbol{O}_2 = 2L\hat{\boldsymbol{u}}$ with $2L < \sigma$. The dipoles $\boldsymbol{\mu}_1$ and $\boldsymbol{\mu}_2$ are chosen such that $\boldsymbol{\mu}_a \cdot \hat{\boldsymbol{u}} = 0$ and we set

$$\begin{cases} \boldsymbol{\mu}_1 = \mu \hat{\boldsymbol{\mu}}_1 \\ \boldsymbol{\mu}_2 = \lambda\mu (\cos \alpha \hat{\boldsymbol{\mu}}_1 + \sin \alpha (\hat{\boldsymbol{\mu}}_1 \times \hat{\boldsymbol{u}})) \end{cases} \quad (1)$$

where the parameters $\alpha \in [-\pi, \pi]$ and $0 \leq \lambda \leq 1$ define the second dipole $\boldsymbol{\mu}_2$ from the dipole $\boldsymbol{\mu}_1$ and the axis $\hat{\boldsymbol{u}}$. We name *Rectus (R-) bidipolar hard sphere* (R_α -HS) for $0 < \alpha < \pi$ and *Sinister (S-) bidipolar hard sphere* (S_α -HS) for $-\pi < \alpha < 0$

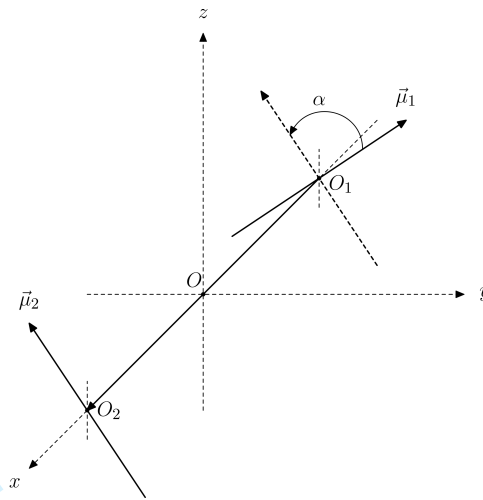


Figure 1. Representation the molecule-fixed local frame for the Sinister bidipolar hard sphere enantiomer (S_α -HS). The frame is defined from vectors $\hat{\mathbf{u}}$, $\boldsymbol{\mu}_1$ and $\boldsymbol{\mu}_2$ via Eqs.(1-3) ; $|\mathbf{O}_1\mathbf{O}_2| = 2L < \sigma$. The thick dashed vector is the projection of $\boldsymbol{\mu}_2$ in the plane $(O_1, \hat{\mathbf{e}}_z, \boldsymbol{\mu}_1)$.

(see figure 1). In this nomenclature, it is clear that $R_{(-\alpha)}$ -HS \equiv S_α -HS ; molecules R_α -HS and S_α -HS are enantiomers.

Chiral parameters or chiral indices have been introduced to give a quantitative measure of the chirality of a molecule [20, 54]. In particular, A.B. Harris and co-workers [54] have defined chiral parameters as pseudoscalars constructed from the structure of molecules described via the representation theory of the three-dimensional rotation group $O(3)$; they have also related chiral parameters to the cholesteric pitch of generic liquid crystal models. For the chiral dipolar hard sphere model, we may define a pseudoscalar from the three vectors $\hat{\mathbf{u}}$, $\boldsymbol{\mu}_1$ and $\boldsymbol{\mu}_2$ as

$$\chi = L\hat{\mathbf{u}} \cdot (\boldsymbol{\mu}_2 \times \boldsymbol{\mu}_1) = L\lambda\mu^2 \sin \alpha \quad (2)$$

and take χ as the chiral parameter of this model ; we have $\chi(S_\alpha - HS) = -\chi(R_\alpha - HS)$. If $\chi = 0$, then both enantiomers are equivalent and the bidipolar hard sphere model is achiral. This occurs if one of the following conditions is verified : (a) $L = 0$, then both point dipoles are located at the center of the sphere and the model reduces to the dipolar hard sphere model ; (b) $\lambda = 0$, in this case, there is only one point dipole in the molecule and (c) $\sin \alpha = 0$ then the dipoles and the molecular axis are all in the same plane which is a plane of symmetry for the molecule.

A physical interpretation to $|\chi^*| = 1$ is less obvious ; to obtain $|\chi^*| = 1$ one needs to have $\lambda = 1$, thus a symmetry is restored and then the chirality is perhaps less marked for these particular cases with $\lambda = 1$ (for instance, see below subsection 2.2 and Fig.7). A trivial interpretation of values $|\chi^*| = 1$ would be to say that for these value a maximum discrimination is achieved ; however, this is perhaps not fully correct.

We define the molecule-fixed local frame as

$$\begin{cases} \hat{\mathbf{e}}_z = \frac{\boldsymbol{\mu}_1 + \boldsymbol{\mu}_2}{|\boldsymbol{\mu}_1 + \boldsymbol{\mu}_2|} = \frac{\mathbf{P}}{|\mathbf{P}|} \\ \hat{\mathbf{e}}_x = \hat{\mathbf{u}} \\ \hat{\mathbf{e}}_y = \hat{\mathbf{e}}_z \times \hat{\mathbf{u}} \end{cases} \quad (3)$$

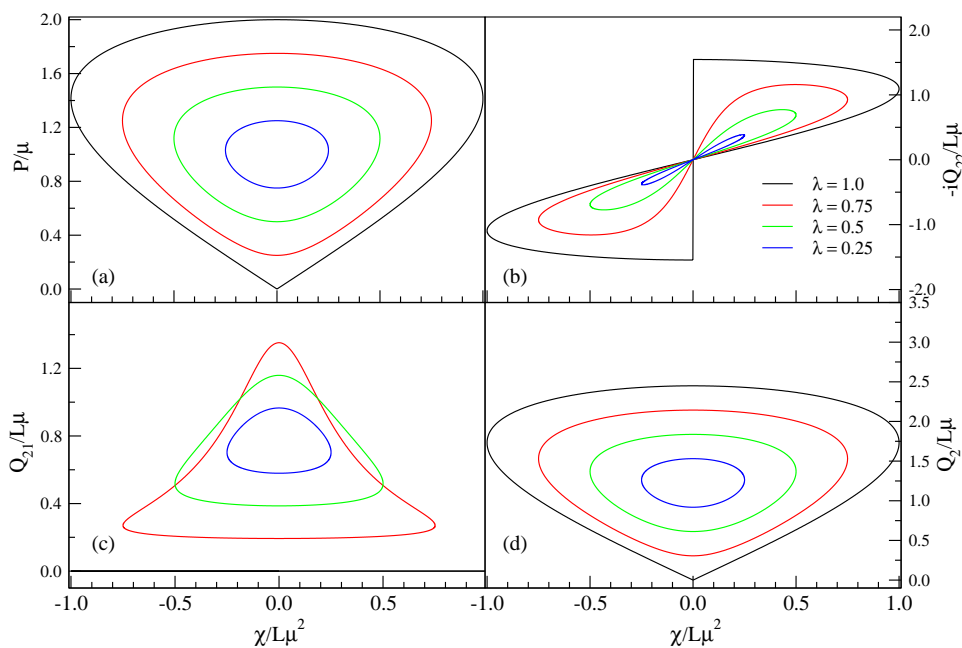


Figure 2. Representation of the spherical components of the dipole and quadrupole moments as function of the chiral parameter χ . The spherical components, represented as function of χ , are multivalued because of the property $\chi(\alpha) = \chi(\pi - \alpha)$ (cf. Eq. (2)). Enantiomers R_α -HS and S_α -HS have equal spherical components when an even symmetry occurs, that is to say for P and Q_{21} . One may note that for $\lambda = 1$ one has $Q_{21} = 0$.

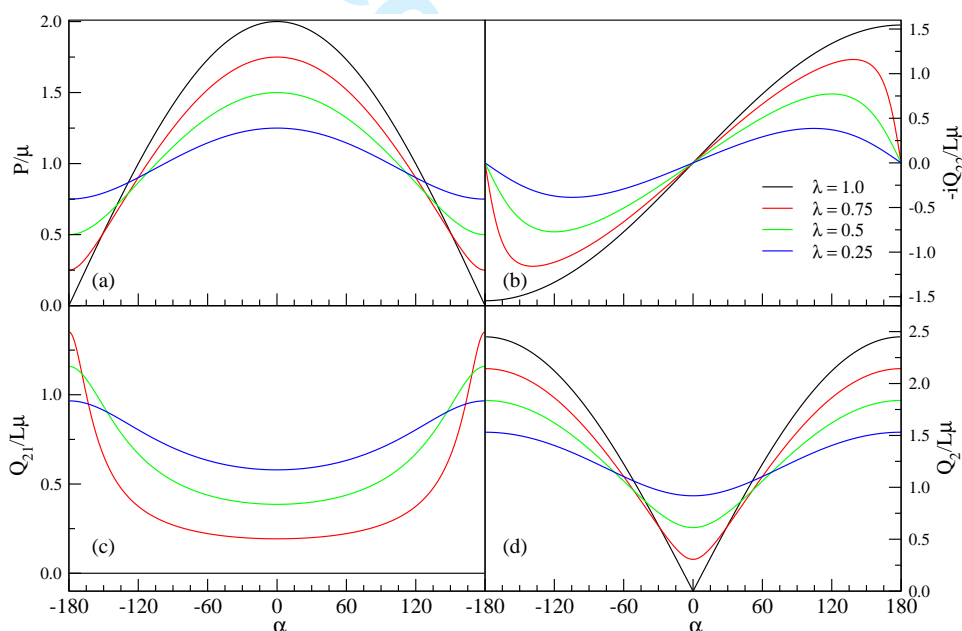


Figure 3. Representation of the spherical components of the dipole and quadrupole as function of α . As shown below, the knowledge of P , Q_{21} and Q_{22} as function of the parameters of the model determine fully all components of the spherical multipole tensor of an arbitrary order l (see below).

where \mathbf{P} is the total dipole of the molecule. In this molecule-fixed frame, the projections of the dipoles onto the frame axis are given by

$$\begin{cases} \mu_1 = \mu(1 + 2\lambda \cos \alpha + \lambda^2)^{-1/2} [-\lambda \sin \alpha \hat{e}_y + (1 + \lambda \cos \alpha) \hat{e}_z] \\ \mu_2 = \mu(1 + 2\lambda \cos \alpha + \lambda^2)^{-1/2} [\lambda \sin \alpha \hat{e}_y + \lambda(\cos \alpha + \lambda) \hat{e}_z] \\ \mathbf{P} = \mu(1 + 2\lambda \cos \alpha + \lambda^2)^{1/2} \hat{e}_z \end{cases} \quad (4)$$

It is worthwhile to note that the total dipole of enantiomers R_α -HS and S_α -HS in the molecule-fixed frame are the same, we have $\mathbf{P}(R_\alpha\text{-HS}) \equiv \mathbf{P}(S_\alpha\text{-HS})$. One should note also that $\mathbf{P} = 0$ can be obtained only if $\lambda = 1$ and $\alpha = \pi$, then $\chi = 0$ and the model is achiral ; thus, all chiral bi-dipolar hard sphere have a non-zero net total dipole.

The dipole distribution of the chiral hard sphere may be written as

$$\boldsymbol{\mu}(\mathbf{r}) = \boldsymbol{\mu}_1\delta(\mathbf{r} + L\hat{\mathbf{u}}) + \boldsymbol{\mu}_2\delta(\mathbf{r} - L\hat{\mathbf{u}}) \quad (5)$$

and from multipole expansion for any dipolar distribution (see appendix A), the cartesian components of the quadrupole moment are given by

$$[q] = \frac{3}{2} \frac{L\mu}{\sqrt{1 + 2\lambda \cos \alpha + \lambda^2}} \begin{bmatrix} 0 & 2\lambda \sin \alpha (\lambda^2 - 1) \\ 2\lambda \sin \alpha & 0 & 0 \\ (\lambda^2 - 1) & 0 & 0 \end{bmatrix} \quad (6)$$

and spherical components by

$$\begin{cases} Q_{22} = i\sqrt{\frac{15}{2\pi}} \frac{L\lambda\mu \sin \alpha}{\sqrt{1 + 2\lambda \cos \alpha + \lambda^2}} \\ Q_{21} = \sqrt{\frac{15}{8\pi}} \frac{L\mu(1 - \lambda^2)}{\sqrt{1 + 2\lambda \cos \alpha + \lambda^2}} \\ Q_{20} = 0 \end{cases} \quad (7)$$

For enantiomers, we have $Q_{22}(R_\alpha\text{-HS}) \equiv -Q_{22}(S_\alpha\text{-HS})$ and $Q_{21}(R_\alpha\text{-HS}) \equiv Q_{21}(S_\alpha\text{-HS})$. The magnitude of the quadrupole is [53]

$$\hat{Q}_2^2 = \frac{4\pi}{5} \sum_m |Q_{2m}|^2 = \frac{3}{2} L^2 \mu^2 \left[\frac{4\lambda^2 \sin^2 \alpha + (1 - \lambda^2)^2}{1 + 2\lambda \cos \alpha + \lambda^2} \right] \quad (8)$$

Obviously, one has $\hat{Q}_2^2(R_\alpha\text{-HS}) = \hat{Q}_2^2(S_\alpha\text{-HS})$. In Eq.(8), it might be surprising to find $\hat{Q}_2^2 \neq 0$ for $\lambda = 0$, since there is only a single dipole in the hard sphere in these cases. This stems from dependence on the choice of the origin in the computation of the quadrupole (the single dipole is shifted by $-L\hat{\mathbf{u}}$ from the center of the hard sphere - see also ref.[53], p.69). This origin dependence highlight the fact that when setting $\lambda = 0$, the chiral bidipolar hard sphere model do not reduce to the classical dipolar hard sphere model. On Figs.(2-3), we show the dipole and quadrupole components as functions of the chiral parameter χ and angle α ; on these representations, the influence of chirality is related to odd or even properties of the function. As shown on Fig.2-3, a difference between enantiomers R_α and S_α is found only in Q_{22} .

The spherical components of the octopole are given by

$$\begin{cases} Q_{33} = 0 \\ Q_{32} = \frac{1}{2} \sqrt{\frac{105}{8\pi}} L^2 \mu (1 + 2\lambda \cos \alpha + \lambda^2)^{1/2} = \frac{1}{2} \sqrt{\frac{35}{2}} L^2 Q_{10} \\ Q_{31} = 0 \\ Q_{30} = -\frac{3}{2} \sqrt{\frac{7}{4\pi}} L^2 \mu (1 + 2\lambda \cos \alpha + \lambda^2)^{1/2} = -\frac{\sqrt{21}}{2} L^2 Q_{10} \end{cases} \quad (9)$$

and its magnitude is

$$\hat{Q}_3^2 = \frac{4\pi}{7} \sum_m |Q_{3m}|^2 = \frac{33}{8} L^4 \mu^2 (1 + 2\lambda \cos \alpha + \lambda^2) = \frac{11\pi}{2} L^4 Q_{10}^2 \quad (10)$$

It is apparent also on Eqs.(9-10) that the octopole moments are the same for both enantiomers. More generally, by using Eq.(5) and the definition of the spherical component of multipoles Eq.(A4), we found

$$\frac{Q_{ll}}{\mu L^{(l-1)}} = il \frac{\lambda \sin \alpha}{\sqrt{1 + 2\lambda \cos \alpha + \lambda^2}} (1 + (-1)^l) Y_{ll}(\hat{e}_x) \quad (11)$$

and, for $0 \leq m \leq l - 1$, we have

$$\begin{aligned} \frac{Q_{lm}}{\mu L^{(l-1)}} = & -\sqrt{(l+m+1)(l-m)} \left[\frac{(\lambda^2 - (-1)^l) + (1 - (-1)^l) \lambda \cos \alpha}{\sqrt{1 + 2\lambda \cos \alpha + \lambda^2}} \right] Y_{l(m+1)}(\hat{e}_x) \\ & + im \frac{\lambda \sin \alpha}{\sqrt{1 + 2\lambda \cos \alpha + \lambda^2}} (1 + (-1)^l) Y_{lm}(\hat{e}_x) \end{aligned} \quad (12)$$

The value of $Y_{lm}(\hat{e}_x)$ may be easily computed, it comes

$$Y_{lm}(\hat{e}_x) = \sqrt{\frac{2l+1}{4\pi}} \begin{cases} (-1)^{(l+m)/2} \frac{[(l-m)!(l+m)!]^{1/2}}{(l-m)!!(l+m)!!} & \text{for } (l+m) \text{ even} \\ 0 & \text{for } (l+m) \text{ odd} \end{cases} \quad (13)$$

therefore, only one of the two contributions in the right handed side of Eq.(12) gives Q_{lm} . From this computation, we see that all spherical components can be

computed only from Q_{10} , Q_{21} and Q_{22} ; more precisely, from Eqs.(11-12), we have

$$\left\{ \begin{array}{l} \frac{Q_{ll}}{\mu L^{(l-1)}} = l(1 + (-1)^l) \sqrt{\frac{2\pi}{15}} \left(\frac{Q_{22}}{\mu L} \right) Y_{ll}(\hat{e}_x) \\ \frac{Q_{lm}}{\mu L^{(l-1)}} = (1 + (-1)^l) \sqrt{\frac{8\pi}{15}} \left[\frac{\sqrt{(l+m+1)(l-m)}}{2} \left(\frac{Q_{21}}{\mu L} \right) Y_{l(m+1)}(\hat{e}_x) \right. \\ \left. + m \left(\frac{Q_{22}}{\mu L} \right) Y_{lm}(\hat{e}_x) \right] \\ - \frac{(1 - (-1)^l)}{2} \sqrt{(l+m+1)(l-m)} \sqrt{\frac{4\pi}{3}} \left(\frac{Q_{10}}{\mu} \right) Y_{l(m+1)}(\hat{e}_x) \end{array} \right. \quad (14)$$

Since $R_{(-\alpha)}$ -HS \equiv S_{α} -HS, we have

$$Q_{lm}(R_{\alpha}) - Q_{lm}(S_{\alpha}) = 2(1 + (-1)^l) m L^{(l-2)} \sqrt{\frac{2\pi}{15}} Q_{22} Y_{lm}(\hat{e}_x) \quad (15)$$

thus, all spherical components of multipoles of enantiomers R_{α} -HS and S_{α} -HS are equal, but those with l and m even and $m \neq 0$. It is worthwhile to note that Q_{lm} is proportional to only one of the three components Q_{10} , Q_{21} or Q_{22} , because of Eq.(13). Eq.(14) shows that the behavior of all components of multipoles are given (up to a numerical multiplicative factor) by Figs.(2 -3) as functions of the model parameters ; in particular the difference $Q_{lm}(R_{\alpha}) - Q_{lm}(S_{\alpha})$ is given in Fig.2(b), as function of χ , and in Fig.3(b), as function of α .

As shown in Eq.(14) all components of the multipoles dependent only on the three components Q_{10} , Q_{21} or Q_{22} , therefore it is advantageous to define the three reduced geometrical parameters χ^* , P^* and r^* as

$$\left\{ \begin{array}{l} \chi^* = \frac{\chi}{L\mu^2} = \lambda \sin \alpha \\ P^* = \frac{P}{\mu} = (1 + 2\lambda \cos \alpha + \lambda^2)^{1/2} \\ r^* = \frac{r}{L\mu} = (1 - \lambda^2) \end{array} \right. \quad (16)$$

2.2. Interaction energies between two enantiomers.

The interaction energy between two enantiomers can be computed in two ways. First, by summing up all interaction energies due to dipole-dipole interactions and/or, second, by using the multipole expansion. In the next section, we give some preliminary numerical results obtained with Monte Carlo Metropolis sampling of the phase space ; in these computations, all dipole-dipole interactions are taken into account explicitly and long ranged interactions are computed with the Ewald method [51, 55].

In the present subsection, we give some analytical results for the interaction energy between two enantiomers by using the multipole expansion when $r \gg \sigma > 2L$ and we give also some analytical and numerical results obtained by computing explicitly all dipole-dipole interactions between two enantiomers at contact (*i.e.*

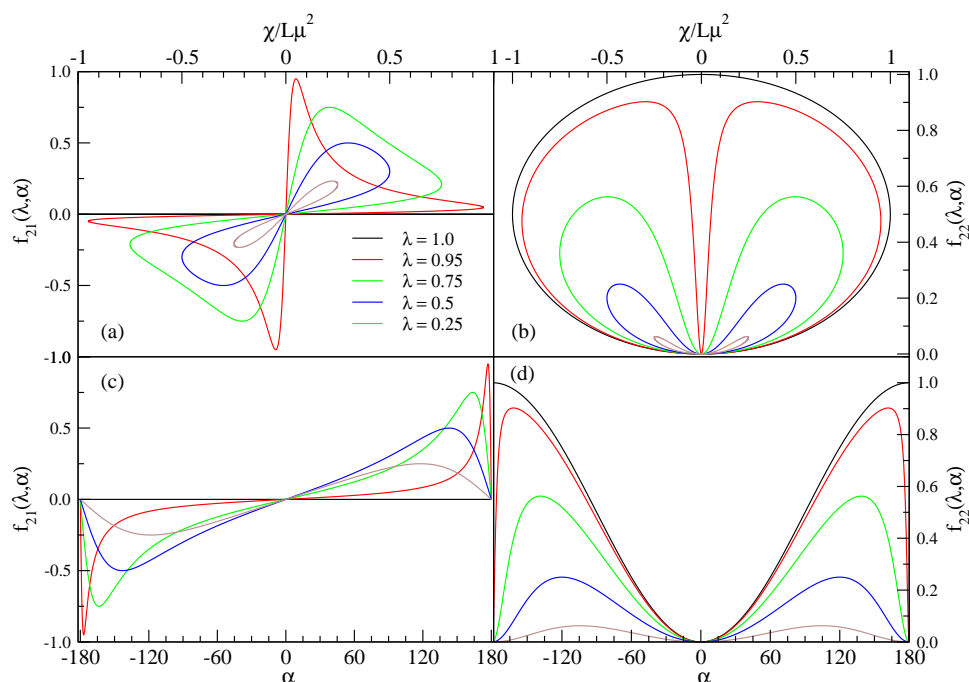


Figure 4. Representation of the two functions f_{21} and f_{22} as function of the reduced chiral parameter $\chi^* = \chi/L\mu^2$ and as functions of α .

enantiomer.

The quadrupole-quadrupole interaction contributes also to $\Delta U^{(LU)}$; $\Delta U_{22}^{(LU)}$ may be written as

$$\Delta U_{22}^{(LU)} = -\frac{3}{2} \left(\frac{L^2 \mu^2}{r^5} \right) f_{22}(\lambda, \alpha) \left[A_0 + 20A_1 + 30\sqrt{2}A_2 + 140A_3 + 35A_4 \right] - 6 \left(\frac{L^2 \mu^2}{r^5} \right) f_{21}(\lambda, \alpha) \left[B_0 + \frac{5}{\sqrt{2}}B_1 - 5\sqrt{2}B_2 - \frac{35}{4}B_3 \right] \quad (21)$$

with the functions f_{22} and f_{21} describing the dependence of $\Delta U_{22}^{(LU)}$ on the model parameters; these two functions are given by

$$\begin{cases} f_{22}(\lambda, \alpha) = \frac{\lambda^2 \sin^2 \alpha}{(1 + 2\lambda \cos \alpha + \lambda^2)} = \frac{\chi^{*2}}{P^{*2}} \\ f_{21}(\lambda, \alpha) = \frac{(1 - \lambda^2)\lambda \sin \alpha}{(1 + 2\lambda \cos \alpha + \lambda^2)} = \frac{r^* \chi^*}{P^{*2}} \end{cases} \quad (22)$$

In Figs.4 (a,b), we represent these two functions versus the chiral parameter χ and, in Figs.4 (c,d) as functions of α .

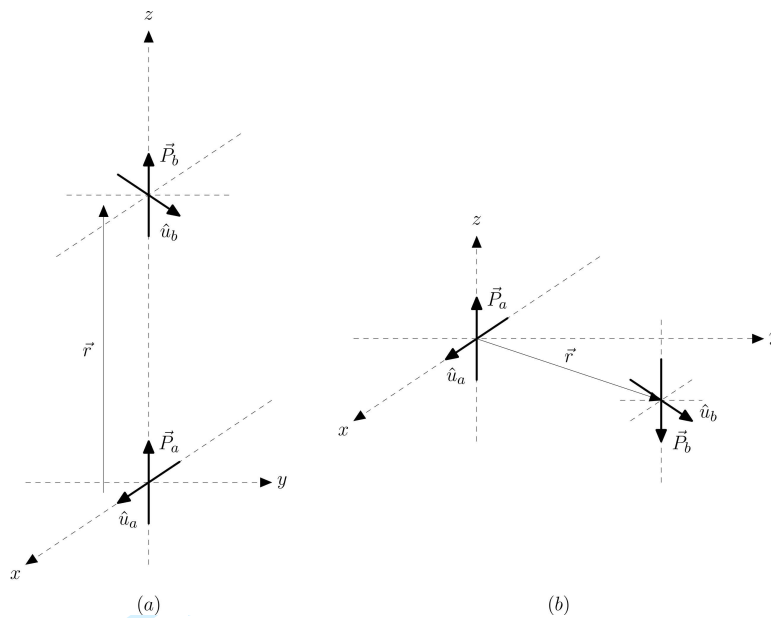


Figure 5. Configurations of particular interest in dipolar system. (a) Colinear aligned total dipole moments, these kind of configurations between two dipolar particle is responsible for chains formation at low temperature and low density : for this configuration, one has $\theta = 0$ and $\theta_2 = 0$. (b) Antiparallel total dipole moment : for this configuration, one has $\theta = \pi/2$ and $\theta_2 = \pi$.

The functions A and B depend on orientations ω_2 and ω . More precisely, we have

$$\left\{ \begin{array}{l} A_0 = (35 \cos^4 \theta - 30 \cos^2 \theta + 3)[(1 + \cos^2 \theta_2) \sin 2\chi_2 \sin 2\phi_2 - 2 \cos \theta_2 \cos 2\chi_2 \cos 2\phi_2] \\ A_1 = \sin \theta (7 \cos^3 \theta - 3 \cos \theta) \sin \theta_2 [\cos 2\chi_2 \cos(\phi_2 + \phi) - \cos \theta_2 \sin 2\chi_2 \sin(\phi_2 + \phi)] \\ A_2 = \sin^2 \theta (7 \cos^2 \theta - 1) \sin 2\phi \sin^2 \theta_2 \sin 2\chi_2 \\ A_3 = \sin^3 \theta \cos \theta \sin \theta_2 [\cos 2\chi_2 \cos(\phi_2 - 3\phi) - \cos \theta_2 \sin 2\chi_2 \sin(\phi_2 - 3\phi)] \\ A_4 = \sin^4 \theta [2 \cos \theta_2 \cos 2\chi_2 \cos(2\phi_2 - 4\phi) - (1 + \cos^2 \theta_2) \sin 2\chi_2 \sin(2\phi_2 - 4\phi)] \end{array} \right. \quad (23)$$

and

$$\left\{ \begin{array}{l} B_0 = (35 \cos^4 \theta - 30 \cos^2 \theta + 3) \sin \theta_2 [\cos 2\chi_2 \cos \phi_2 + \cos \theta_2 \cos 2\chi_2 \cos \phi_2] \\ B_1 = \sin \theta (7 \cos^3 \theta - 3 \cos \theta) [(1 + \cos^2 \theta_2) \sin 2\chi_2 \sin(2\phi_2 - \phi) \\ \quad + 2 \cos \theta_2 \cos 2\chi_2 \cos(2\phi_2 - \phi) - \frac{3}{2\sqrt{2}} \sin^2 \theta_2 \sin 2\chi_2 \cos \phi] \\ B_2 = \sin^2 \theta (7 \cos^2 \theta - 1) \sin \theta_2 [\cos 2\chi_2 \sin(\phi_2 - 2\phi) + \cos \theta_2 \sin 2\chi_2 \sin(\phi_2 - 2\phi)] \\ B_3 = \sin^3 \theta \cos \theta [(1 + \cos^2 \theta_2) \sin 2\chi_2 \sin(2\phi_2 - 3\phi) - 2 \cos \theta_2 \cos 2\chi_2 \cos(2\phi_2 - 3\phi)] \end{array} \right. \quad (24)$$

Obviously, if the distance between two enantiomers is too small the multiple expansion ceases to be accurate, however, the interaction energy between enantiomers may still be computed by summing all dipole-dipole interactions. The total interaction energy between two enantiomers a and b has thus to be written as

$$E^{(a,b)} = E^{(1a,1b)} + E^{(1a,2b)} + E^{(2a,1b)} + E^{(2a,2b)} \quad (25)$$

12

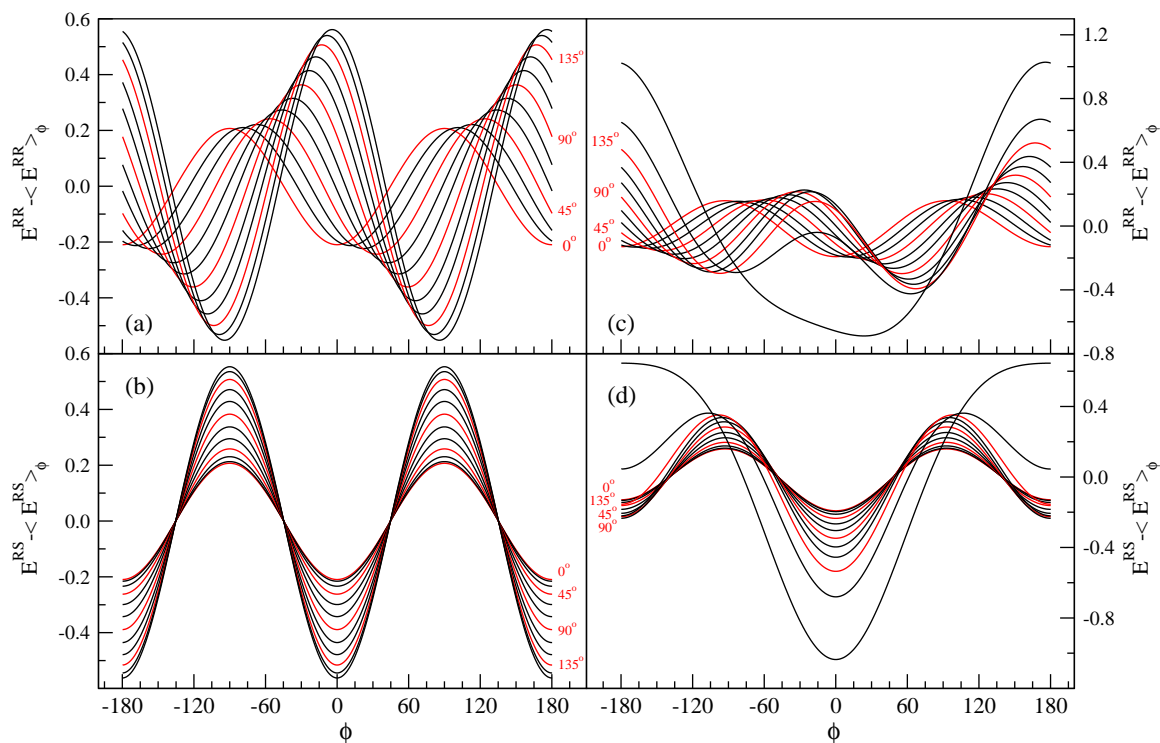


Figure 6. Interaction energies for two enantiomers in configurations given by Fig.5 (a) at contact $z = \sigma$. The angle ϕ is defined by $\cos \phi = \hat{\mathbf{u}}_a \cdot \hat{\mathbf{u}}_b$. In all computations reported in these figures, $\mu = 1.0$, $L = 0.25\sigma$ and the curves correspond to an increase in the value of α by 15° ; the red lines correspond to $\alpha = 0^\circ$, 45° , 90° and 135° , these values are indicated at edge of curves in figures. The energy $\langle E^{XY} \rangle_{\phi}$ is the average energy over the orientation $\hat{\mathbf{u}}_b$ of enantiomer Y. (a) X and $Y \equiv R_\alpha$ and $\lambda = 1.0$; (b) $Y \equiv S_\alpha$ and $\lambda = 1.0$; (c) X and $Y \equiv R_\alpha$ and $\lambda = 0.75$ and (d) $Y \equiv S_\alpha$ and $\lambda = 0.75$.

Table 1. Average energy over the orientation $\hat{\mathbf{u}}_b$ of enantiomers Y and location ϕ_m of the orientation of $\hat{\mathbf{u}}_b$, for which the minimum energy is reached, when $Y \equiv R_\alpha$ for configurations given by Fig.5 (a) at contact $z = \sigma$.

α	$\langle E^{XY} \rangle_{\phi}$		ϕ_m	
	$\lambda = 1$	$\lambda = 0.75$	$\lambda = 1$	$\lambda = 0.75$
0°	-5.794	-4.436	0°	0°
15°	-5.695	-4.362	11.2°	10.4°
30°	-5.506	-4.145	22.4°	20.8°
45°	-4.945	-3.800	33°	31°
60°	-4.345	-3.350	43°	40.2°
75°	-3.647	-2.825	51.6°	48.4°
90°	-2.897	-2.263	59.2°	55.4°
105°	-2.147	-1.701	65.8°	61°
120°	-1.448	-1.177	71.4°	65.2°
135°	-0.848	-0.727	76.6°	67°
150°	-0.388	-0.381	81.2°	62.8°
165°	-0.098	-0.164	85.6°	11°

where $E^{(ia,jb)}$ denotes the interaction energy between the dipole i of enantiomer a with dipole j of enantiomer b ; it is given by

$$E^{(ia,jb)} = \frac{1}{|\mathbf{r}_{ab}^{ij}|^3} \left[\boldsymbol{\mu}_i^{(a)} \cdot \boldsymbol{\mu}_j^{(b)} - 3(\boldsymbol{\mu}_i^{(a)} \cdot \hat{\mathbf{r}}_{ab}^{ij})(\boldsymbol{\mu}_j^{(b)} \cdot \hat{\mathbf{r}}_{ab}^{ij}) \right] \quad (26)$$

and the distance vectors between point dipoles are

$$\begin{cases} \mathbf{r}_{ab}^{11} = \mathbf{r} + L(\hat{\mathbf{u}}_a - \hat{\mathbf{u}}_b) \\ \mathbf{r}_{ab}^{12} = \mathbf{r} + L(\hat{\mathbf{u}}_a + \hat{\mathbf{u}}_b) \\ \mathbf{r}_{ab}^{21} = \mathbf{r} - L(\hat{\mathbf{u}}_a + \hat{\mathbf{u}}_b) \\ \mathbf{r}_{ab}^{22} = \mathbf{r} - L(\hat{\mathbf{u}}_a - \hat{\mathbf{u}}_b) \end{cases} \quad (27)$$

Even for simple relative configurations, as the ones shown on Fig.5(a-b), the total interaction energy between two enantiomers is a bit complicated when computed by summing all dipole-dipole interactions. For instance, the interaction energy between two R_α enantiomers in a configuration given by Fig.5(a) is

$$\begin{aligned} E^{(a,b)} &= \frac{\mu^2}{|z|^3} \\ &\times \left\{ \frac{1}{\left(1 + 2\left(\frac{L^2}{z^2}\right)(1 - \cos\phi)\right)^{5/2}} \left[\left(P^{*2} + \frac{r^{*2}}{P^{*2}}\right) \left(\left(\frac{L}{z}\right)^2 (1 - \cos\phi) - 1\right) \right. \right. \\ &- 6\left(\frac{L}{z}\right) \chi^* \sin\phi + 2\left(\frac{\chi^{*2}}{P^{*2}}\right) \left(\cos\phi - \left(\frac{L}{z}\right)^2 (2 - 2\cos\phi + \sin^2\phi)\right) \left. \right] \\ &+ \frac{1}{\left(1 + 2\left(\frac{L^2}{z^2}\right)(1 + \cos\phi)\right)^{5/2}} \left[\left(P^{*2} - \frac{r^{*2}}{P^{*2}}\right) \left(\left(\frac{L}{z}\right)^2 (1 + \cos\phi) - 1\right) \right. \\ &\left. \left. + 6\left(\frac{L}{z}\right) \chi^* \sin\phi - 2\left(\frac{\chi^{*2}}{P^{*2}}\right) \left(\cos\phi - \left(\frac{L}{z}\right)^2 (2 + 2\cos\phi + \sin^2\phi)\right) \right] \right\} \quad (28) \end{aligned}$$

where $\cos\phi = \hat{\mathbf{u}}_a \cdot \hat{\mathbf{u}}_b$ and (χ^*, P^*, r^*) given by Eq.(16). The chirodiastaltic interaction between enantiomers R_α and S_α , computed by summing the four dipole-dipole interaction energies, for the configuration given on Fig.5(a) is

$$\begin{aligned} \Delta E^{(LU)} &= E(R_\alpha, R_\alpha) - E(R_\alpha, S_\alpha) = \frac{\mu^2}{|z|^3} \\ &\times \left\{ \frac{1}{\left(1 + 2\left(\frac{L^2}{z^2}\right)(1 - \cos\phi)\right)^{5/2}} \left[4\frac{\chi^{*2}}{P^{*2}} \cos\phi - 6\left(\frac{L}{z}\right) \chi^* \sin\phi \right. \right. \\ &- 4\left(\frac{L^2}{z^2}\right) \frac{\chi^{*2}}{P^{*2}} (\sin^2\phi + 2 - 2\cos\phi) \left. \right] \\ &+ \frac{1}{\left(1 + 2\left(\frac{L^2}{z^2}\right)(1 + \cos\phi)\right)^{5/2}} \left[-4\frac{\chi^{*2}}{P^{*2}} \cos\phi + 6\left(\frac{L}{z}\right) \chi^* \sin\phi \right. \\ &\left. \left. - 4\left(\frac{L^2}{z^2}\right) \frac{\chi^{*2}}{P^{*2}} (\sin^2\phi + 2 + 2\cos\phi) \right] \right\} \quad (29) \end{aligned}$$

14

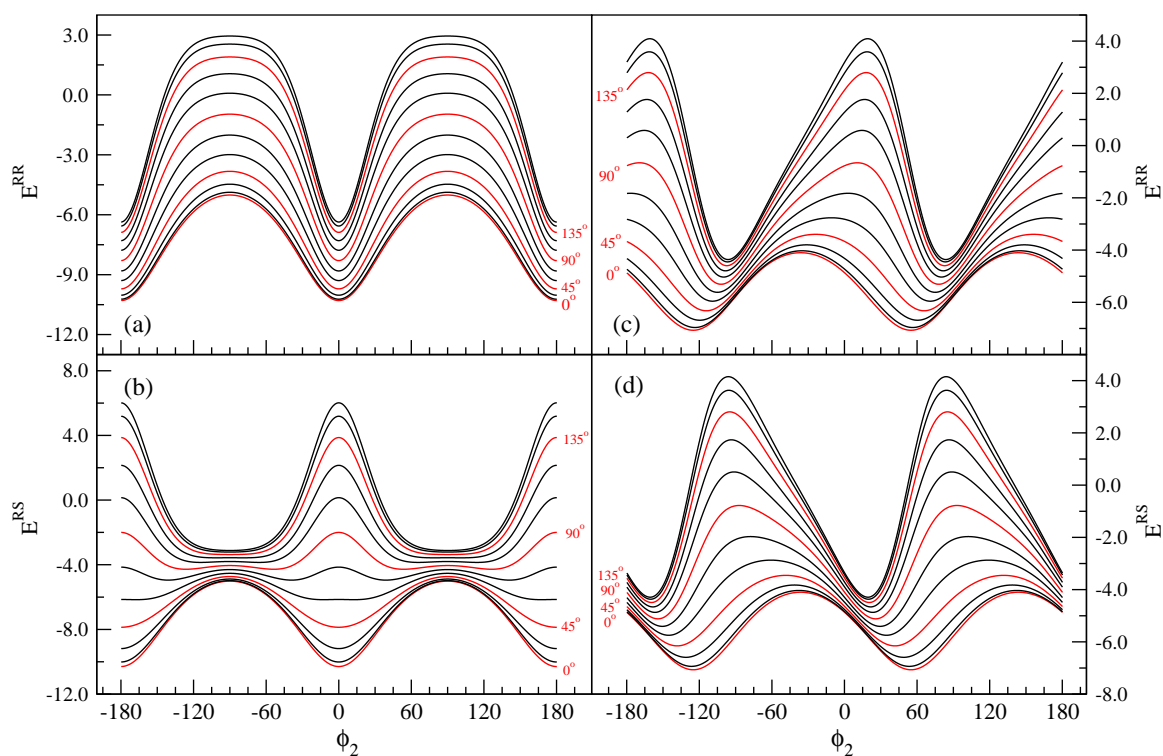


Figure 7. Interaction energies for two enantiomers in configurations given by Fig.5 (b) at contact $r = \sigma$ for $\lambda = 1$. In all computation, $\mu = 1.0$, $L = 0.25\sigma$ and notations are the same as in Fig.6. For the configuration given by Fig.5 (b), the angle ϕ is defined by $\cos \phi = \hat{\mathbf{u}}_a \cdot \hat{\mathbf{r}}$ and the angle ϕ_2 by $\cos \phi_2 = \hat{\mathbf{u}}_a \cdot \hat{\mathbf{u}}_b$. (a-b) : $\phi = 0^\circ$ and (c-d) : $\phi = 45^\circ$.

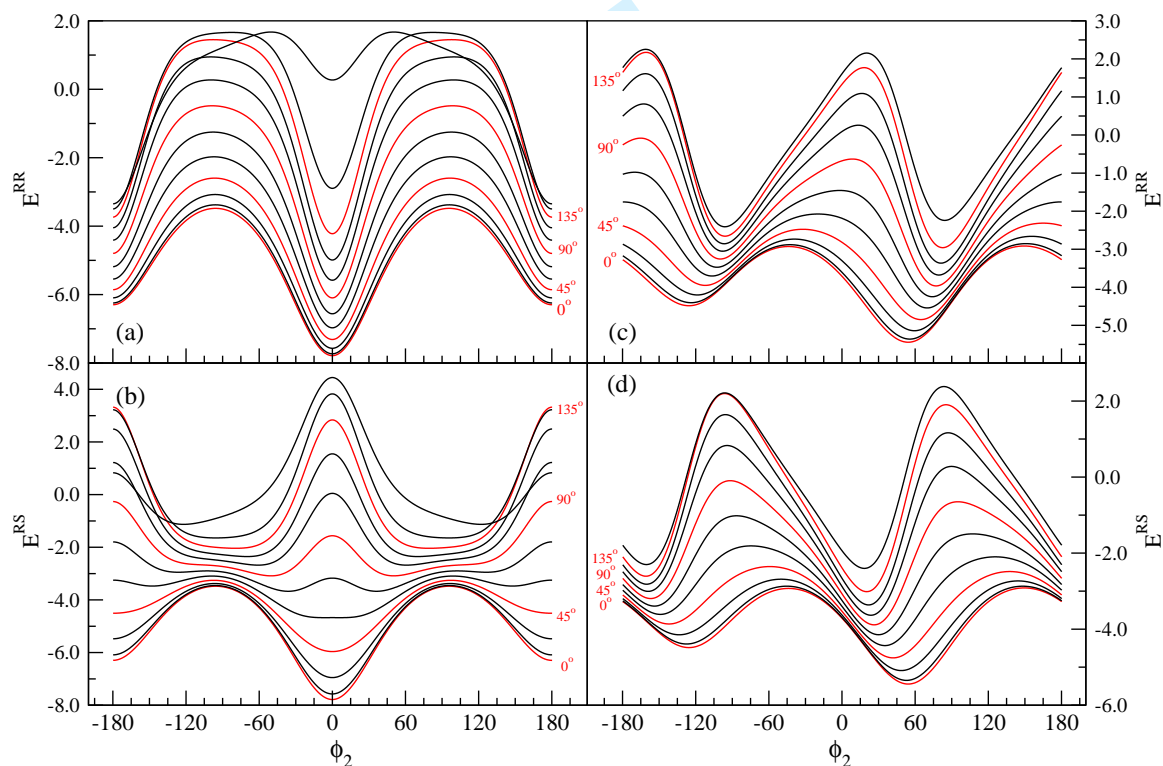


Figure 8. Interaction energies between two enantiomers in configurations given by Fig.5 (b) at contact $r = \sigma$ for $\lambda = 0.75$. Notations are the same as for Fig.7.

For $|z| \gg L$, a Taylor expansion of Eq.(29) gives

$$\begin{aligned} \Delta E^{(LU)} &= \frac{\mu^2}{|z|^3} \left[24 \frac{\chi^{*2}}{P^{*2}} \left(\frac{L^2}{z^2} \right) \sin 2\phi - 60\chi^* \left(\frac{L^3}{z^3} \right) \sin \phi + o\left(\frac{L^4}{z^4}\right) \right] \\ &= \Delta U_{22}^{(LU)}(\theta_2 = 0, \theta = 0) + \Delta U_{32}^{(LU)}(\theta_2 = 0, \theta = 0) + o\left(\frac{L^4 \mu^2}{z^7}\right) \end{aligned} \quad (30)$$

where we have set $\phi = \phi_2 + \chi_2$ in Eqs.(23-24) to obtain $\Delta U_{22}^{(LU)}$. Subtracting Eq.(30) from Eq.(29), may allow to check the degree of accuracy of the multipole expansion for the configuration of Fig.5 (a).

On Figs.6, we represent interaction energies for enantiomers in the colinear aligned total dipole moment configuration (Fig.5-a). These energies have been computed by summing all dipole interactions between the two enantiomers. To allow simple comparison between interaction energies, for different values of α , we have subtracted to all curves the average, over the orientation \hat{u}_b , of the interaction energy. For all λ , a minimum in the interaction energy between two different enantiomers is always obtained for $\phi = 0$ (\hat{u}_a and \hat{u}_b parallel) ; the anti-parallel configuration of molecular axis \hat{u}_a and \hat{u}_b ($\phi = \pi$) is a relative minimum for the interaction energy for all $\lambda < 1$ (see Fig.6(b-d) - if $\lambda = 1$, the configurations for $\phi = 0$ and $\phi = \pi$ have the same energy) ; one should note also that these minima are relative, because the configurations like in Fig.5 (a) do not permit to reach the smallest distance between two point dipoles. The minimum interaction energy between two enantiomers of same kind is not obtained for parallel or anti-parallel configurations of the molecular axis. The value ϕ_m of the angle for which a minimum interaction energy is obtained, depends on parameters λ and α (see Fig.6(a-c)), several values are given in Table 1 ; average values of $\langle E^{XY} \rangle_\phi$ are also reported in this Table. Therefore, in homochiral systems (systems that are composed with exclusively one enantiomer) with a large enough total dipole moment and in thermodynamical conditions where dipolar systems form chains [56, 58], we may observe formation of chains too, and the molecular axis of the enantiomers may have helical arrangement. Addition of chiral enantiomers in the system will reduce the range of the helical arrangement in the chains. For $\lambda = 1$, the minimum at $\phi = \phi_m$ has the same value than the one found at $\phi = \phi_m - \pi$, therefore *right* and *left-handed* helical arrangement of the molecular axis in the chains will compete in homochiral systems.

For the configuration given in Fig.5(b) and for $r \gg L$ ($\theta = \pi/2$ and $\theta_2 = \pi$), the multipole-multipole chirodiastaltic interaction is found as

$$\begin{aligned} \Delta E^{(LU)} &= -3 \frac{\mu^2}{r^3} \left[4 \left(\frac{L}{r} \right) \chi^* \sin(\phi_2 - \phi - 2\chi_2) \right. \\ &\quad \left. + \left(\frac{L^2}{r^2} \right) \frac{\chi^{*2}}{P^{*2}} (3 \cos 2(\phi_2 - \chi_2) - 35 \cos 2(\phi_2 - \chi_2 - 2\phi)) \right] + o\left(\frac{L^3 \mu^2}{z^6}\right) \\ &= \Delta U_{12}^{(LU)}(\theta_2 = \pi, \theta = \frac{\pi}{2}) + \Delta U_{22}^{(LU)}(\theta_2 = \pi, \theta = \frac{\pi}{2}) + o\left(\frac{L^3 \mu^2}{z^6}\right) \end{aligned} \quad (31)$$

On Figs.7 and 8, we represent interaction energies for enantiomers in the antiparallel total dipole configurations (Fig.5-b) for $\phi = 0$ and $\pi/4$. On Figs.7 (a,c) and 8 (a,c), we represent interactions energies between two R_α enantiomers for $\lambda = 1$ and 0.75 and on Figs.7 (b,d) and 8 (b,d) we represent interactions energies between

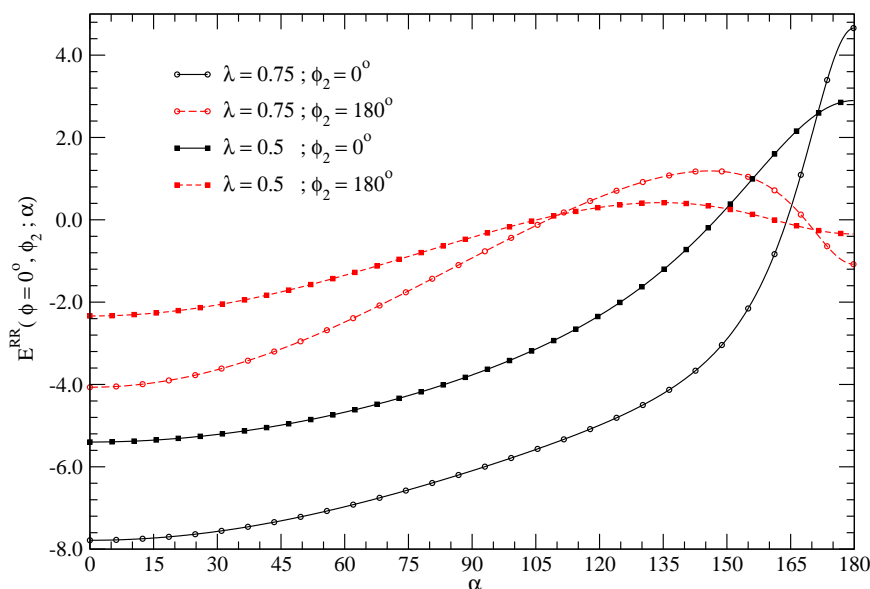


Figure 9. Relative minimum of interaction energies between two enantiomers R_α in antiparallel total dipole configurations with $\phi = 0$ as functions of α . Open circles correspond to $\lambda = 0.75$ and filled squares to $\lambda = 0.5$, the black solid lines are for $\phi_2 = 0$ and the red dashed lines for $\phi_2 = \pi$. For $\lambda = 0.75$, one has $\alpha_m \simeq 166^\circ$ and for $\lambda = 0.5$, $\alpha_m \simeq 150^\circ$.

enantiomers R_α and S_α . The coupling between ϕ and ϕ_2 renders quite complicated the energy landscape of antiparallel configurations. The relative minima for antiparallel configurations (Fig.5-b) are smaller than the minima found for colinear configurations (Fig.5-a), therefore the colinear and antiparallel configurations are in drastic competition by comparison to dipolar hard sphere systems.

For two identical enantiomers, when $\phi = n\pi/2$ (with $n = -1, 0, 1$ or 2), the location of minimum interaction energies are independent on α . For instance, if $\phi = 0$, the relative minima for two R_α enantiomers are always obtained for $\phi_2 = 0$ or π ; if $\lambda = 1$, these two minima have the same value, but if $\lambda < 1$ the two minima are not equivalent and their value dependent on α . On Fig.9, we give the value of the minimum energy for $\phi = 0$ and $\phi_2 = 0$ or π for $\lambda = 0.75$ and 0.5 ; as shown on this figure for values of $\alpha > \alpha_m(\lambda)$ the configuration $\phi_2 = \pi$ is more stable than the configuration $\phi_2 = 0$. The amplitude of variation of interaction energies with ϕ_2 are larger for antiparallel configurations than variation with ϕ for aligned colinear configurations.

The locations of relative minimum interaction energies between enantiomers R_α and S_α depend not only on ϕ and ϕ_2 , but also on α . For instance on Fig.7(b) ($\phi = 0$) and for $\alpha = 5\pi/12$ (75°), we found four different minima located at $\phi_2 \simeq \pm 141^\circ$ and $\pm 39^\circ$.

The computations of interaction energies between two chiral dipolar hard spheres show that a lot of different configurations may be in competition, even for simple configurations as the ones shown on Figs.5. In the next section, we give some preliminary results obtained with Monte Carlo simulations for several cases.

3. Preliminary Monte Carlo results

As shown in the previous section, interaction energies between two enantiomers as function of their relative orientation may have a lot of relative minima; therefore, despite the apparent simplicity of the model, the thermodynamical properties chiral dipolar hard sphere systems are quite complicated. In particular, because the

energy landscape of the interaction between two enantiomers shows large variations, one may predict that frustration phenomena will play an important role in phases at low densities, low temperatures and also in solid phases.

We define the reduced quantities as follow : for volume of the simulation box $V^* = V/\sigma^3$, density $\rho^* = \rho\sigma^3 = N\sigma^3/V$, pressure $p^* = p\sigma^2/kT$ and dipole moment $\mu^* = (\mu/kT\sigma^3)^{1/2}$. For a given model of enantiomer, defined by (λ, α) and L , the reduced total dipole moment P^* of the molecule is related to μ^* according to Eq.(4). In all computations, we have chosen $L^* = L/\sigma = 1/4$ as in the numerical computations done in the previous section (see Figs.6-8). At the end of this section, a short discussion on the influence of L on structures is presented ; this influence is illustrated on two cases : $L^* = 0.025$ and $L^* = 0.425$. For notational convenience the asterisks will be drop in the following.

Mixtures of enantiomers R_α -HS and S_α -HS are also of interest, we define densities $\rho_R = N_R/V$ and $\rho_S = N_S/V$ respectively for enantiomers R_α -HS and S_α -HS and the ratio $X = \rho_S/\rho_R = N_S/N_R$. The ratio X is related to the *enantiomeric excess* (ee) in enantiomer R_α -HS by $ee = 1 - X$. In the following, we have considered only two mixtures of enantiomers : homochiral R_α systems ($X = 0$) and racemic R_α - S_α systems ($X = 1$).

Monte Carlo simulations have been performed in canonical (NVT) and isobaric (NPT) ensembles with system size $N = N_R + N_S = 512$ or 1000. Periodic boundary conditions are used and dipolar interaction energies between two enantiomers is computed with Eqs.(25-27) where long ranged contributions are taken into account by using the Ewald method [51].

From a technical point of view, as a consequence of the numerous number of relative minima in interaction energies, the convergence of the Monte Carlo algorithm and the sampling of the phase space will require a large number of MC cycles (one MC cycle corresponds, on average, to one trial move per particle for NVT simulations ; for NPT simulation, an additional trial move of the volme of the box is done every MC-cycle). For most results presented in this section, between 5×10^4 and 10^5 MC cycles have been achieved for the relaxation and convergence from an initial condition and averages have been accumulated over about 10^5 and 2×10^5 MC cycles, respectively for systems with 1000 and 512 particles.

Periodic boundary conditions are used and interaction energies are computed with the Ewald method [51] by summing all dipole-dipole interactions between enantiomers. The average energy U is computed as

$$U = \left\langle \sum_{a \neq b} E^{(a,b)} \right\rangle \quad (32)$$

where $E^{(a,b)}$ is the interaction energy between enantiomers a and b Eqs.(25-27) and $\langle . \rangle$ is the average of the MC sampling. Some computation have been done with an external electric field $\mathbf{E}_0 = E_0 \hat{e}_z$, the energy in the external field is computed as

$$V = \left\langle - \sum_{a=1}^N \mathbf{P}^{(a)} \cdot \mathbf{E}_0 \right\rangle = \left\langle - \sum_{a=1}^N (\boldsymbol{\mu}_1^{(a)} + \boldsymbol{\mu}_2^{(a)}) \cdot \mathbf{E}_0 \right\rangle \quad (33)$$

Table 2. Average energies and eigenvalues S_+ , S_0 and S_- for homochiral- R_α and racemic systems in external electric field $\mathbf{E} = E\hat{e}_z$ ($E = 10$) obtained in canonical (NVT) Monte Carlo simulations. The numbers in brackets give the accuracy on the last digit of the averages. For all systems $N = 512$, $\mu = 1.0$ and $\rho = 0.05$ (or $\rho = 0.5$). The parameters α and λ define the molecular structure of enantiomers as given by Eq.(1).

α	Homochiral			Racemic			S_+	S_0	S_-	
	$\beta U/N$	$\beta V/N$	S_+	S_0	S_-	$\beta U/N$				$\beta V/N$
$\lambda = 1$										
20°	-5.3(2)	-18.83(5)	0.25(1)	0.18(1)	-0.442(4)	-5.3(3)	-18.85(6)	0.27(2)	0.18(2)	-0.442(4)
35°	-4.2(2)	-18.18(6)	0.24(1)	0.19(1)	-0.434(4)	-4.1(3)	-18.19(6)	0.25(2)	0.18(2)	-0.435(4)
45°	-3.0(3)	-17.55(6)	0.24(1)	0.19(1)	-0.429(4)	-2.9(2)	-17.54(6)	0.25(2)	0.18(2)	-0.429(4)
55°	-2.2(1)	-16.79(6)	0.25(1)	0.18(1)	-0.424(4)	-2.2(1)	-16.79(6)	0.24(2)	0.19(2)	-0.424(4)
60°	-1.9(1)	-16.37(6)	0.24(1)	0.19(1)	-0.423(5)	-1.9(1)	-16.37(6)	0.24(2)	0.18(2)	-0.423(4)
90°	-0.83(5)	-13.17(5)	0.23(1)	0.17(1)	-0.405(6)	-0.82(5)	-13.17(5)	0.23(2)	0.18(2)	-0.404(6)
120°	-0.37(4)	-9.02(5)	0.21(1)	0.16(1)	-0.37(1)	-0.35(3)	-9.01(5)	0.21(2)	0.16(1)	-0.37(1)
150°	-0.21(3)	-4.19(5)	0.16(2)	0.11(2)	-0.27(1)	-0.18(3)	-4.19(4)	0.16(1)	0.11(1)	-0.27(1)
$\lambda = 0.95$										
170°	-0.11(2)	-0.88(3)	0.06(2)	0.02(1)	-0.08(2)	-0.10(2)	-0.88(3)	0.07(1)	0.02(1)	-0.09(2)
$^a 170^\circ$	-1.50(6)	-0.93(3)	0.08(1)	0.03(1)	-0.10(2)	-1.44(6)	-0.91(3)	0.07(1)	0.03(1)	-0.10(1)
$\lambda = 0.75$										
152°	-0.09(2)	-3.89(5)	0.15(1)	0.10(2)	-0.26(1)	-0.09(2)	-3.90(4)	0.16(2)	0.10(2)	-0.26(1)
$^a 152^\circ$	-1.26(5)	-3.96(4)	0.16(2)	0.11(2)	-0.28(1)	-1.21(5)	-3.94(5)	0.16(2)	0.11(2)	-0.27(1)

^a For these computations, the density is $\rho = 0.5$.

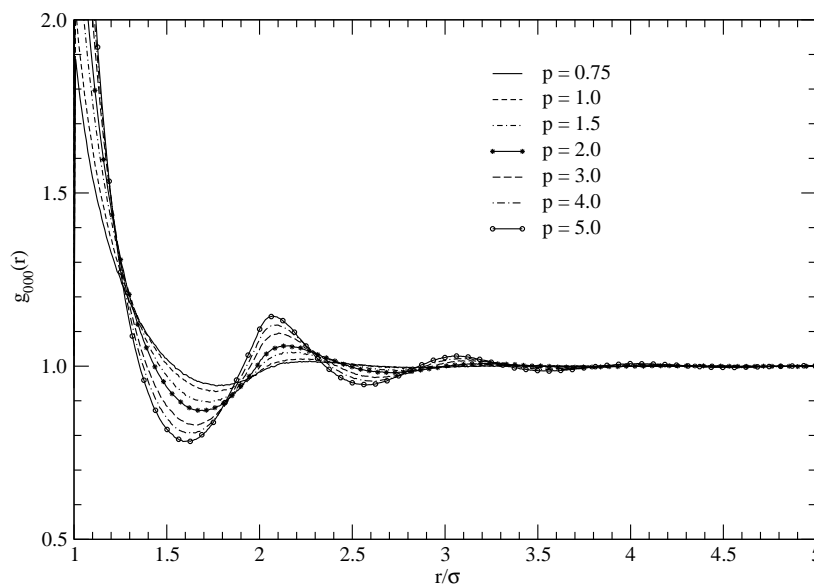


Figure 10. Representation of $g_{000}(r)$ for several value of the pressure obtained by Monte-Carlo sampling of the isobaric (NPT) ensemble of homochiral- R_α systems for $N = 1000$, $\mu = 0.5$, $\alpha = 60^\circ$ and $\lambda = 1.0$.

Possible orientational order can be established by computing the eigenvalues of the tensor

$$Q_{\alpha\beta} = \frac{1}{2N} \sum_{i=1}^N (3\hat{x}_\alpha^i \hat{x}_\beta^i - \delta_{\alpha\beta}) \quad (34)$$

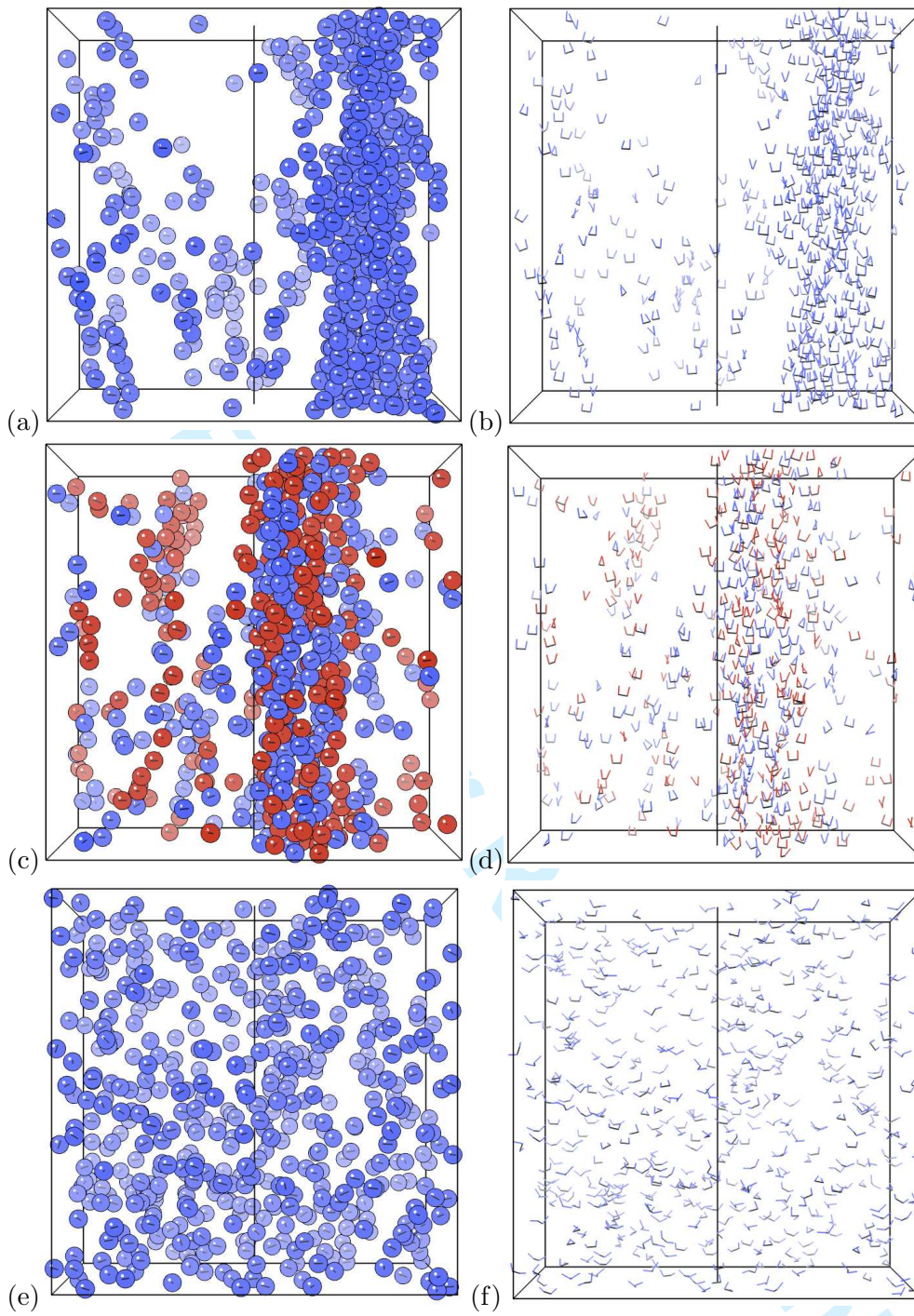


Figure 11. Snapshots of homochiral- R_α and racemic systems in external electric field. For all systems $N = 512$, $\mu = 1.0$, $\rho = 0.05$, $\lambda = 1.0$ and $\mathbf{E} = E\hat{e}_z$ ($E = 10$); the solid vertical line indicates the direction of the field. (a-b): homochiral- R_α with $\alpha = 35^\circ$; (c-d): racemic R_α - S_α system with $\alpha = 35^\circ$ and (e-f) homochiral- R_α with $\alpha = 150^\circ$. R_α -HS enantiomers are represented in blue and S_α -HS enantiomers in red. In (b), (d) and (f), we represent, for the same configurations, molecular axis and segment in the direction of dipoles for each enantiomer; dipoles of R_α -HS enantiomers are represented in blue and dipoles of S_α -HS enantiomers in red.

where \hat{x}_α^i is the cartesian component of a unit vector $\hat{\mathbf{x}}$ of molecule i . The largest eigenvalue S_+ of $Q_{\alpha\beta}$ is used as an order parameter for the isotropic-nematic phase transition in liquid crystals. It is also worthwhile to note that if, all unit vectors $\hat{\mathbf{x}}$ are perpendicular to a given fixed direction then, the eigenvalues are $S_+ = S_0 = 1/4$ and $S_- = -1/2$. In the present work, we have restricted the computation of $Q_{\alpha\beta}$

Table 3. Preliminary results for Monte-Carlo computations in the isobaric (NPT) ensemble of homochiral- R_α systems. These computations are performed with $N = 1000$, $\mu = 0.5$, $\alpha = 60^\circ$ and $\lambda = 1.0$. Notations are the same as in Table 2, p is the reduced pressure and $\langle \rho \rangle$ is the average value of the density.

p	$\langle \rho \rangle$	$\beta U/N$	S_+	S_0	S_-
0.1	0.086(2)	-0.08(1)	0.02(1)	0.00(1)	-0.02(1)
0.25	0.18(3)	-0.17(1)	0.03(1)	0.00(1)	-0.03(1)
0.5	0.29(1)	-0.27(2)	0.02(1)	0.00(1)	-0.02(1)
0.6	0.32(1)	-0.30(2)	0.02(1)	0.00(1)	-0.02(1)
0.75	0.036(1)	-0.34(2)	0.03(1)	0.00(1)	-0.03(1)
0.8	0.37(1)	-0.36(2)	0.04(1)	0.01(1)	-0.03(1)
1.0	0.41(1)	-0.39(2)	0.03(1)	0.00(1)	-0.03(1)
1.5	0.49(2)	-0.48(3)	0.02(1)	0.00(1)	-0.03(1)
2.0	0.55(3)	-0.54(3)	0.02(1)	0.01(1)	-0.03(1)
3.0	0.62(5)	-0.62(6)	0.03(1)	0.01(1)	-0.04(1)
4.0	0.66(6)	-0.7(1)	0.03(1)	0.01(1)	-0.03(1)
5.0	0.70(6)	-0.7(1)	0.02(1)	0.00(1)	-0.02(1)

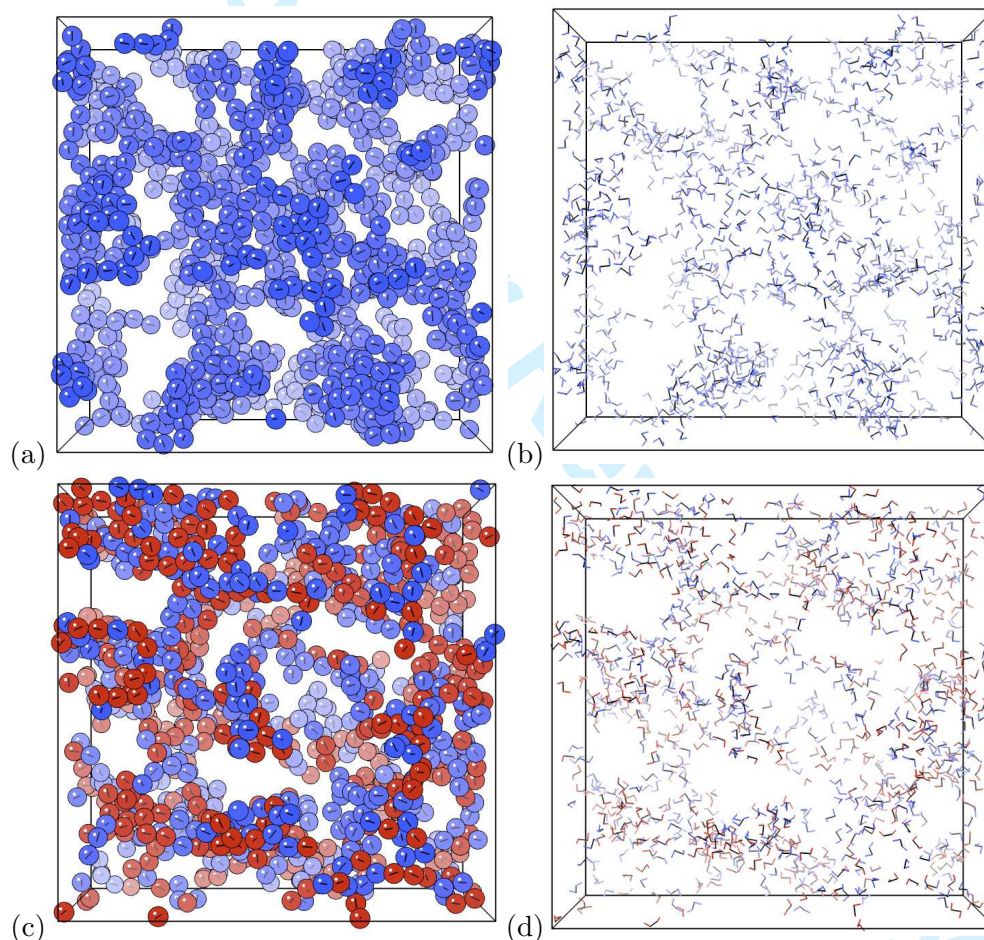


Figure 12. Snapshots of chiral dipolar hard sphere systems for $N = 1000$, $\mu = 2.0$, $\rho = 0.1$, $\alpha = 120^\circ$ and $\lambda = 1.0$. The notations are the same as those in Figs.11. (a-b): homochiral- R_α system ; (c-d): racemic R_α - S_α system. In (a) and (c) hard spheres are represented as balls and molecular axis O_1O_2 by a black segment. No external electric field are applied to the systems.

for the molecular axis \hat{u} of enantiomers.

To study the structure of the systems we have computed the angular projections on rotational invariants of the molecular pair distribution function [59, 61, 73, 74] ; in the present work, we have computed only $g_{000}(r)$, $h_{110}(r)$ and $h_{112}(r)$ for two sets of points and vectors. The first set is the molecule center and the orientation of

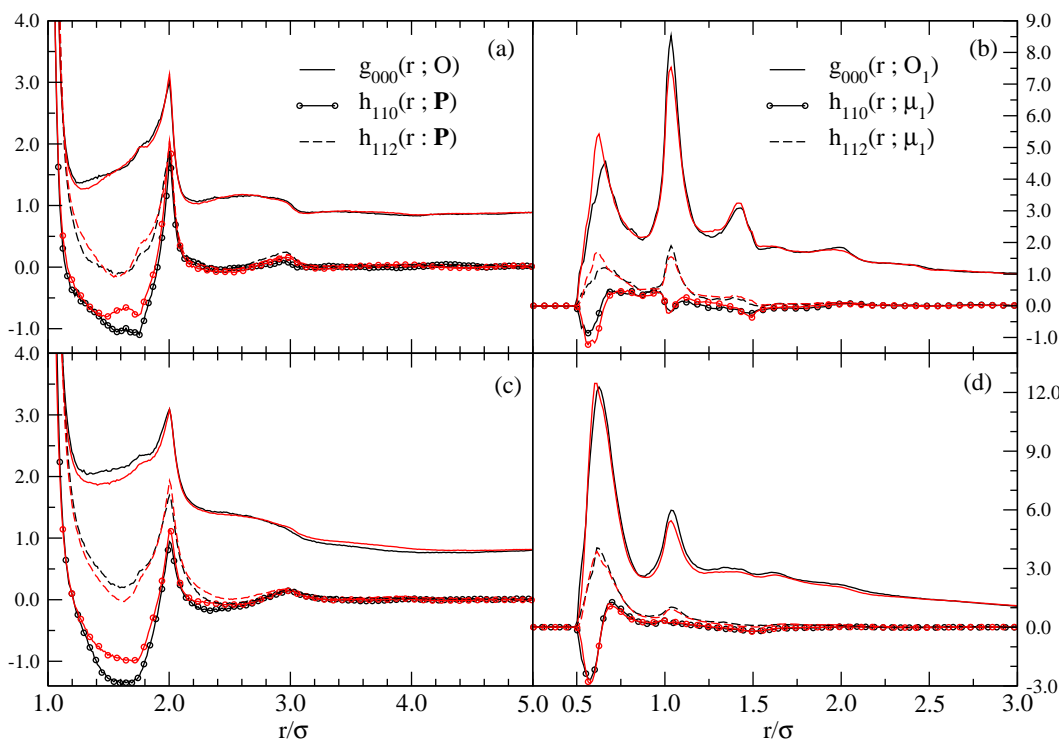


Figure 13. Representation of projections of molecular pair distribution functions computed by Monte Carlo sampling of the (NVT) ensemble of racemic R_α - S_α systems. In these computation, $N = 1000$, $\mu = 1.5$, $\rho = 0.1$ and $\alpha = 30^\circ$; (a-b) $\lambda = 1.0$ and (c-d) $\lambda = 0.75$. The functions represented in (a) and (c) are computed for the set (O, \hat{P}) and the functions represented in (b) and (d) for the set $(O_1, \hat{\mu}_1)$. In all figures, pair distributions functions for *Like-Like* pairs of molecules are represented in black and those for *Like-Unlike* pairs in red.

the total dipole moment : (O, \hat{P}) ; the second set is the site O_1 and the orientation of the dipole μ_1 : $(O_1, \hat{\mu}_1)$. To study the influence of the chirodiastaltic interaction on structure of mixtures of both enantiomers, it will be necessary to compute projections of the pair distribution functions on rotational invariants of higher order since the discriminatory interaction involves dipole-quadrupole interactions.

Table 2, summarizes average energies and eigenvalues of $Q_{\alpha\beta}$ Eq.(34) for homochiral- R_α and racemic systems in external electric field $\mathbf{E} = E\hat{z}$ ($E = 10$), for several values of α and λ . On Table 3, we report some preliminary results of Monte-Carlo computations in the isobaric (NPT) ensemble of homochiral- R_α systems and on Fig.10, we show $g_{000}(r)$ obtained with these computations.

On Fig.11, we give few snapshots of homochiral- R_α and racemic systems in an external field. The results reported on table 2 show that energies and the nematic order parameters for the molecular axis are almost independent on the composition of systems. The eigenvalues S_+ , S_0 and S_- show that on average the molecular axis of enantiomers are perpendicular to the direction of the electric field, this results is quite obvious since the total dipole moment, as defined in Eqs.(3,4), is perpendicular to the molecular axis this tendency decreases as α increases, since the total dipole moment decreases. As shown on the snapshots in Fig.(11), if $\alpha \lesssim 60^\circ$ molecules tend to condense in a large columnar cluster, for both homochiral- R_α and racemic systems in an external electric field (cf. Fig.11 (a-d)); if $\alpha \gtrsim 70^\circ$ the columnar cluster does not form (cf. Fig.11 (e-f)). **There are at least two facts that may help to understand qualitatively the disappearance of the columnar clusters as α increases, while λ and μ are fixed. First, as α increases, the total dipole of each molecule decreases and thus formations of chains in the direction of the external field is less favoured. Second, for large enough α , configurations with two**

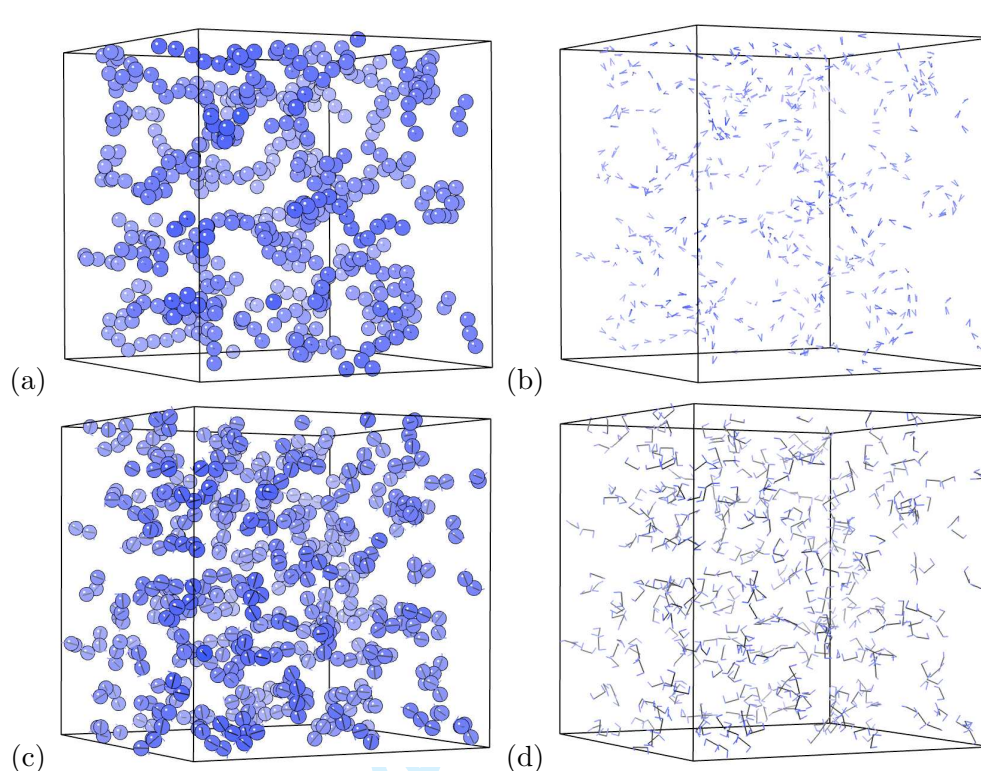


Figure 14. Snapshots of chiral dipolar hard sphere systems for homochiral- R_α system with $N = 512$, $\mu = 1.5$, $\rho = 0.05$, $\alpha = 30^\circ$ and $\lambda = 1.0$ and for two value of L . The notations are the same as those in Figs.11. (a-b): $2L = 0.05\sigma$; (c-d): $2L = 0.95\sigma$. In (a) and (c) hard spheres are represented as balls and molecular axis O_1O_2 by a black segment. No external electric field are applied to the systems.

dipoles belonging to two different molecules may be more easily found, on average, in an antiparallel configuration in a plane perpendicular to the field, while the total dipole of both molecules can still be parallel to the field. At present, it is not clear how the columnar clusters form and which mechanism favour their formation ; further investigations are needed to be conclusive. Homochiral- R_α and racemic R_α - S_α systems in an external electric field exhibit the same properties, however, a close inspection of the snapshots of Fig.11 (a-d) shows that the internal structure of the columnar clusters is not the same in homochiral and racemic systems. In homochiral systems, the molecules in the columnar cluster have an helical arrangement (in agreement with the results shown on Fig.6) ; in racemic systems, these helical arrangement in the columnar clusters are less marked because of the *Like-Unlike* interactions. To obtain more quantitative descriptions of the internal structure of the columnar clusters, some particular order parameters and distribution functions have to be defined.

If there is no external electric field, columnar clusters are not formed instead some complicated structures are formed at low density and large enough μ ; this has occurred for all values of α that have been considered in these preliminary results. On Fig.12, snapshots of homochiral- R_α and racemic R_α - S_α systems are represented, for these systems $\alpha = 120^\circ$ and no external electric fields are applied. Again, in these computations homochiral and racemic systems behave very similarly, however, an inspection of the pair distribution functions show that there is small differences between pair distributions functions for *Like-Like* pairs of molecules and those for *Like-Unlike* pairs (see for instance Fig.13). The comparison between pair distribution functions computed for $\lambda = 1.0$ and 0.75 shows that this parameter have an important influence on the local structure (cf. Fig.13). In particular, when $\lambda \neq 1.0$, interactions between the dipoles μ_1 of two enantiomers are favoured and so an

1 asymmetric arrangement of the molecular axis.

2 There are three important parameters in this chiral model : λ , α and L . So far in
3 this section in the simulations reported (and also in numerical computations done
4 in subsection 2.2), we have set always $L/\sigma = 1/4$ and showed how energy minima
5 and structures depend on λ and α . They will depend also on the ratio L/σ : for
6 instance, if L/σ is small, chains with colinear aligned total dipole moment will be
7 favoured, while, if L/σ is close to 1, structures with colinear aligned molecular axis
8 will be favoured, this behaviour is illustrated on Fig.14.
9

10 11 12 4. Perspectives

13
14 A full determination of the structures and clusters at low densities and temper-
15 atures will require a larger sampling of the phase space ; this can be achieved
16 with longer runs and by implementing trial cluster moves [75–77]. Nematic
17 and helical-cholesteric order parameter and also the bond orientational order
18 parameters [78] will be useful to investigate the properties of structure at low
19 density as function of the *enantiomeric excess* and model parameters, homochiral
20 systems have interest by themselves. Same order parameters and simulations in
21 the isobaric ensemble (NPT) will serve to study the crystal phases of homochiral
22 systems and also as functions of *ee*. Works and computations in these directions
23 are already in progress.
24

25 Another chiral model may be defined from the computation of the multipole
26 moments done in section 2, and in agreement with earlier studies on chiral
27 discrimination due to multipole-multipole interactions [3, 44, 45]. According to
28 Eqs. (4,7), the three components, Q_{10} , Q_{21} and Q_{22} are independent, thus an hard
29 sphere model with dipole-dipole, dipole-quadrupole and quadrupole-quadrupole
30 interactions [79, 80] can be built by using these three multipole components as
31 parameter for the model instead of (λ, α, L) . Such model will be slightly different
32 from the bi-dipolar hard sphere model (and also from the four charges model),
33 since higher order multipole-multipole interactions will not be taken into account
34 in this model. Such systems has not been studied in the present work.
35

36 With the bidipolar model, one may easily build a model of chiral liquid crystal by
37 changing the short ranged steric repulsion by replacing the hard sphere potential
38 by a spherocylinder [81, 82] or ellipsoid hard potential [83, 84], or even by a
39 soft Gay-Berne potential [85, 86]. For these chiral liquid crystal models with two
40 dipoles, all the results of section 2 hold and in particular : the computations of
41 the multipole components and interaction energies between to enantiomers. The
42 modifications of the phase diagram of these systems with the introduction of these
43 chirodiastaltic interactions can be of particular interest for the physics of liquid
44 crystals.
45
46
47
48
49

50 Acknowledgement

51
52 The author acknowledges computation facilities provided by the *Institut du*
53 *Développement et des Ressources en Informatique Scientifique* (IDRIS) under
54 projects 0682104 and 0992104.

55 In the middle of nineties Jean-Jacques was my PhD supervisor ; I have to say that
56 I have been very lucky to benefit of his broad knowledge in the physics of liquids
57 and in computer simulations. Therefore, I am extremely glad to dedicate this paper
58 to Jean-Jacques Weis in this special issue of *Molecular physics* in his honour.
59
60

References

- [1] L. Pasteur, "Études des Phénomènes Relatifs à la Polarisation Rotatoires des Liquides", thesis in chemistry and physics, Faculty of Sciences of Paris (August 23, 1847) ; L. Pasteur "Recherches sur le Dimorphisme", Annales de chimie et de physique, 3 sér., **XXIII**, p.267-294 (1848) ; these two references are reprinted in *Œuvres de Pasteur - Tome Premier : Dissymétrie Moléculaire*, edited by Pasteur Vallery-Radot (Éditions Masson, Paris, 1922).
- [2] R.-S. Cahn, C.-K. Ingold and V. Prelog, *Experientia*, **12**, 81 (1956) ; R.-S. Cahn, *J. Chem. Educ.*, **41**, 116 (1964) ; *Erratum, ibid.*, 508 ; R.-S. Cahn, C.-K. Ingold and V. Prelog, *Ang. Chem.*, **5**, 385 (1966)
- [3] D.P. Craig and D.P. Mellor, *Discriminating Interactions Between Chiral Molecules in Topic in current Chemistry*, **63**, 1 (Springer-Verlag, Berlin, 1976).
- [4] A.A. Kornyshev, D.J. Lee, S. Leikin and A. Wynveen *Rev. Mod. Phys.*, **79**, 943 (2007).
- [5] H. Kuhn, *Curr. Op. Coll. & Int. Sci.*, **13**, 3 (2008).
- [6] R.B. Meyer, L.Liébert, L. Strzelecki and P. Keller, *J. de Physique*, **36**, L69 (1975).
- [7] B.W. van der Meer, G. Vertogen, A.J. Dekker and J.G.J. Ypma, *J. Chem. Phys.*, **65**, 3935 (1976).
- [8] W.J.A. Goossens, *Phys. Rev. A*, **40**, 4019 (1989).
- [9] S. Chandrasekhar, *Liquid Crystals, 2nd ed.*, (Cambridge University Press, Cambridge, 1992).
- [10] P.G. de Gennes and J. Prost, *The Physics of Liquid Crystals, 2nd ed.*, (Clarendon Press, Oxford, 1993).
- [11] R.D. Kamien and J.V. Selinger, *J. Phys.: Condens. Matter*, **13**, R1 (2001).
- [12] A.V. Emelyanenko, A. Fukuda and J.K. Vij, *Phys. Rev. E*, **74**, 011705 (2006).
- [13] J. Xu, R.L.B. Selinger, J.V. Selinger and R. Shashidhar, *J. Chem. Phys.*, **115**, 4333 (2001).
- [14] F. Yan, C. Hixson and D. Earl, *Phys. Rev. Lett.*, **101**, 157801 (2008).
- [15] W.H. de Jeu, B.I. Ostrovskii and A.N. Shalaginov, *Rev. Mod. Phys.*, **75**, 181 (2003).
- [16] M.A. Osipov, H. Stegemeyer and A. Sprick, *Phys. Rev. E*, **54**, 6387 (1996).
- [17] M. Čepič, *Europhys. Lett.*, **75**, 771 (2006).
- [18] W. Kuhn, *Trans. Farraday Soc.*, **26**, 293 (1930).
- [19] D.J. Caldwell and H. Eyring, *The Theory of Optical Activity.*, (New-York, Wiley Interscience, 1971).
- [20] M.A. Osipov, B.T. Pickup and D.A. Dunmur, *Mol. Phys.*, **84**, 1193 (1995).
- [21] X.-O. Wang, J.-Q. Li and C.-F. Li, *Chem. Phys.*, **320**, 37 (2005).
- [22] X.-O. Wang, L.-J. Gong and C.-F. Lei, *J. Chem. Phys.*, **129**, 074708 (2008).
- [23] J.J. Maki and A. Persoons, *J. Chem. Phys.*, **104**, 9340 (1996).
- [24] J. Trost and K. Hornberger, *Chem. Phys.*, **335**, 115 (2007).
- [25] E.B. Barros *et al*, *Phys. Rep.*, **431**, 261 (2006).
- [26] M.P. Anantram and F.Léonard *Rep. Prog. Phys.*, **69**, 507 (2006).
- [27] J. Charlier, X. Blase and S. Roche, *Rev. Mod. Phys.*, **79**, 677 (2007).
- [28] D.J. Lee, A. Wynveen and A.A. Kornyshev, *Phys. Rev. E*, **70**, 051913 (2004).
- [29] G.M. Grason and R.F. Bruinsma, *Phys. Rev. E*, **76**, 021924 (2007).
- [30] D.P. Craig and D. P. Mellor [3] have chosen the term *chirodiastaltic* ('diastaltic' \equiv 'serving to distinguish') because of its explicit reference to chirality. Another terminology *diastereotopic* has been introduced by B. Bosnich and D.W. Watts B. Bosnich and D.W. Watts, *Inorg. Chem.*, **14**, 47 (1975).
- [31] L. D. Barron and C. J. Johnston, *Mol. Phys.*, **42**, 33 (1981).
- [32] J. K. Jenkins, A. Salam and T. Thirunamachandran, *Mol. Phys.*, **82**, 835 (1994).
- [33] D.K. Yang and P.P. Crooker, *Phys. Rev. A*, **35**, 4419 (1987).
- [34] G.T. Evans, *Mol. Phys.*, **77**, 969 (1992).
- [35] A. Ferrarini, G.J. Moro and P.L. Nordio, *Mol. Phys.*, **87**, 485 (1996).
- [36] R. Berardi, M. Cecchini and C. Zannoni, *J. Chem. Phys.*, **119**, 9933 (2003).
- [37] M. Cao and P.A. Monson, *J. Chem. Phys.*, **122**, 054505 (2005).
- [38] J. Peón, J. Saucedo-Zugazagoitia, F. Pucheta-Mendez, R.A. Perusquia, G. Sutmann and J. Quintana-H, *J. Chem. Phys.*, **125**, 104908 (2006).
- [39] I. Paci and N.M. Cann, *J. Chem. Phys.*, **115**, 8489 (2001).
- [40] I. Paci, J. Dunford and N.M. Cann, *J. Chem. Phys.*, **118**, 7519 (2003).
- [41] I. Paci and N.M. Cann, *J. Chem. Phys.*, **120**, 4816 (2004).
- [42] Y. Huh and N.M. Cann, *J. Chem. Phys.*, **121**, 10299 (2004).
- [43] R. Memmer, *J. Chem. Phys.*, **114**, 8210 (2001).
- [44] D.P. Craig and P.E. Schipper, *Chem. Phys. Lett.*, **25**, 476 (1974).
- [45] D.P. Craig and P.E. Schipper, *Proc. R. Soc. London, Ser. A*, **342**, 19 (1975).
- [46] An example of an achiral model of dipolar hard spheres possessing two colinear dipoles is given in the reference : P.J. Camp and G.N. Patey, *Phys. Rev. E*, **60**, 4280 (1999).
- [47] A.V. Luzanov and L.N. Lisetskii *J. Struct. Chem.*, **42**, 544 (2001).
- [48] C.A. Bosello and R. Nibbi, *Math. Meth. Appl. Sci.*, **26**, 375 (2003).
- [49] A. Salam, *J. Chem. Phys.*, **124**, 014302 (2006).
- [50] J. Choi and M.Cho, *J. Chem. Phys.*, **127**, 024507 (2007).
- [51] J.-J. Weis and D. Levesque, *Advanced Computer Simulation Approaches for Soft Matter Sciences II*, edited by C. Holm and K. Kremer, Advances in Polymer Science Vol. 185 (Springer, New York, 2005).
- [52] J.D. Jackson, *Classical Electrodynamics, 2nd ed.* (Wiley, New York, 1975)
- [53] C.G. Gray and K.E. Gubbins, *Theory of molecular fluids. Volume 1: Fundamentals.* (Clarendon Press, Oxford, 1984).
- [54] A.B. Harris, R.D. Kamien and T.C. Lubensky, *Rev. Mod. Phys.*, **71**, 1745 (1999).
- [55] De Leeuw, S.W., Perram, J.W., and Smith, E.R., 1980, *Proc. R. Soc. Lond. A*, **373**, 27 ; *ibid*, 57.
- [56] J.-J. Weis and D. Levesque, *Phys. Rev. Lett.*, **71**, 2729 (1993).
- [57] J.-J. Weis and D. Levesque, *Phys. Rev. E*, **48**, 3728 (1993).
- [58] D. Levesque and J.-J. Weis, *Phys. Rev. E*, **49**, 5131 (1994).
- [59] E. Lomba, F. Lado and J.-J. Weis, *Phys. Rev. E*, **61**, 3838 (2000).
- [60] J.-J. Weis, *Mol. Phys.*, **100**, 579 (2002).
- [61] J.-J. Weis, J.M. Tavares and M.M. Telo da Gama, *J. Phys: Condens. Matter*, **14**, 9171 (2002).

- 1 [62] J.M. Tavares, J.-J. Weis and M.M. Telo da Gama, *Phys. Rev. E*, **65**, 061201 (2002).
2 [63] J.-J. Weis, *J. Phys: Condens. Matter*, **15**, S1471 (2003).
3 [64] M.J. Fernaudo, E. Lomba, J.-J. Weis and D. Levesque, *Mol. Phys.*, **101**, 1721 (2003).
4 [65] M.J. Fernaudo, E. Lomba, C. Martin, D. Levesque and J.-J. Weis *J. Chem. Phys.*, **119**, 364 (2003).
5 [66] J.-J. Weis, *Mol. Phys.*, **103**, 7 (2005).
6 [67] J.-J. Weis, *J. Chem. Phys.*, **123**, 044503 (2005).
7 [68] C. Holm and J.-J. Weis, *Curr. Op. Coll. & Int. Sci.*, **10**, 133 (2005).
8 [69] J.M. Tavares, J.-J. Weis and M.M. Telo da Gama, *Phys. Rev. E*, **73**, 041507 (2006).
9 [70] J.-J. Weis and D. Levesque, *J. Chem. Phys.*, **125**, 034504 (2006).
10 [71] C. Alvarez, M. Mazars and J.-J. Weis, *Phys. Rev. E*, **77**, 051501 (2008).
11 [72] J. Richardi, M.P. Pileni and J.-J. Weis, *Phys. Rev. E*, **77**, 061510 (2008).
12 [73] M.S. Wertheim, *J. Chem. Phys.*, **55**, 4291 (1971).
13 [74] L. Blum and A.J. Torruella, *J. Chem. Phys.*, **56**, 303 (1972).
14 [75] D. Frenkel, *Proc. Natl. Acad. Sci. U.S.A.*, **101**, 51 (2004).
15 [76] S. Whitelam and P.L. Geissler, *J. Chem. Phys.*, **127**, 154101 (2007).
16 [77] N.G. Almarza and E. Lomba, *J. Chem. Phys.*, **127**, 084116 (2007).
17 [78] D.R. Nelson and J. Toner, *Phys. Rev. B*, **24**, 363 (1981) ; P.J. Steinhardt, D.R. Nelson and M.
18 Ronchetti, *Phys. Rev. B*, **28**, 784 (1983).
19 [79] A. Aguado and P.A. Madden, *J. Chem. Phys.*, **119**, 7471 (2003).
20 [80] T. Laino and J. Hutter, *J. Chem. Phys.*, **129**, 074102 (2008).
21 [81] J. Vieillard-Baron, *J. Chem. Phys.*, **56**, 4729 (1972).
22 [82] D. Frenkel and B.M. Mulder, *Mol. Phys.*, **55**, 1171 (1985) ; *ibid.*, 1193 (1985).
23 [83] J. Vieillard-Baron, *Mol. Phys.*, **28**, 809 (1974).
24 [84] J.A.C. Veerman and D. Frenkel, *Phys. Rev. A*, **41**, 3237 (1990) ; *ibid.*, **43**, 1193 (1985).
25 [85] J.G. Gay and B.J. Berne, *J. Chem. Phys.*, **74**, 3316 (1981).
26 [86] E. de Miguel, L.F. Rull and K.E. Gubbins, *Phys. Rev. A*, **44**, 3813 (1992)

Appendix A. Multipole expansion for a dipole distribution.

In this appendix, we give general formulas for the multipole expansion of a dipole distribution $\boldsymbol{\mu}(\mathbf{r})$ located in a finite region Ω of the space. From classical electromagnetism theory [52, 53] and choosing the origin inside Ω , the electrostatic potential $\Phi(\mathbf{r})$, due to the dipole distribution in Ω , is given by

$$\begin{aligned}\Phi(\mathbf{r}) &= \int_{\Omega} \frac{\boldsymbol{\mu}(\mathbf{r}') \cdot (\mathbf{r} - \mathbf{r}')}{|\mathbf{r} - \mathbf{r}'|^3} d\mathbf{r}' = - \int_{\Omega} \boldsymbol{\mu}(\mathbf{r}') \cdot \nabla_{\mathbf{r}} \left(\frac{1}{|\mathbf{r} - \mathbf{r}'|} \right) d\mathbf{r}' \\ &= \int_{\Omega} \boldsymbol{\mu}(\mathbf{r}') \cdot \nabla_{\mathbf{r}'} \left(\frac{1}{|\mathbf{r} - \mathbf{r}'|} \right) d\mathbf{r}'\end{aligned}\quad (\text{A1})$$

Since we are interested in the potential at \mathbf{r} outside the dipole distribution, we set $r > r'$ and $\hat{\mathbf{r}}'$ and $\hat{\mathbf{r}}$, the unitary vectors that define directions of \mathbf{r}' and \mathbf{r} . The relation

$$\frac{1}{|\mathbf{r} - \mathbf{r}'|} = \sum_{l=0}^{\infty} \sum_{m=-l}^{m=l} \left(\frac{4\pi}{2l+1} \right) \frac{r'^l}{r^{(l+1)}} Y_{lm}(\hat{\mathbf{r}}') Y_{lm}^*(\hat{\mathbf{r}}) \quad (\text{A2})$$

is reported in Eq.(A1) and the multipole expansion for a dipole distribution is given by

$$\Phi(\mathbf{r}) = \sum_{l=0}^{\infty} \sum_{m=-l}^{m=l} \left(\frac{4\pi}{2l+1} \right) Q_{lm} \frac{Y_{lm}^*(\hat{\mathbf{r}})}{r^{(l+1)}} \quad (\text{A3})$$

with Q_{lm} the m^{th} component of the spherical multipole moment tensor of order l defined by

$$Q_{lm} = \int_{\Omega} \boldsymbol{\mu}(\mathbf{r}') \cdot \nabla_{\mathbf{r}'} \left[r'^l Y_{lm}(\hat{\mathbf{r}}') \right] d\mathbf{r}' \quad (\text{A4})$$

Eqs. (A3-A4) are the multipole expansion for a dipole distribution. In the following, we give explicitly the Q_{lm} up to $l = 3$ for any dipole distribution. From Eq.(A4), and since any dipole distribution can also be represented as a real charge density, it is easy to show that

$$Q_{l,-m} = (-1)^m Q_{l,m}^* \quad (\text{A5})$$

A.1. The total charge in Ω : Q_{00} .

From Eq.(A4), we have

$$Q_{00} = \int_{\Omega} \boldsymbol{\mu}(\mathbf{r}) \cdot \nabla_{\mathbf{r}} \left[Y_{00}(\hat{\mathbf{r}}) \right] d\mathbf{r} = 0 \quad (\text{A6})$$

Of course, this result is obvious for any dipole distribution.

A.2. The dipole moment tensor : Q_{1m} .

The components Q_{11} and Q_{10} are given by

$$\begin{cases} Q_{11} = -\sqrt{\frac{3}{8\pi}} \left(\int_{\Omega} \boldsymbol{\mu}(\mathbf{r}) \cdot \nabla_{\mathbf{r}} [r \sin \theta e^{i\phi}] d\mathbf{r} \right) \\ Q_{10} = \sqrt{\frac{3}{4\pi}} \left(\int_{\Omega} \boldsymbol{\mu}(\mathbf{r}) \cdot \nabla_{\mathbf{r}} [r \cos \theta] d\mathbf{r} \right) \end{cases} \quad (\text{A7})$$

thus, we find

$$\begin{cases} Q_{11} = -\sqrt{\frac{3}{8\pi}} [P_x + iP_y] \\ Q_{10} = \sqrt{\frac{3}{4\pi}} P_z \end{cases} \quad (\text{A8})$$

Where \mathbf{P} is the total dipole in Ω given by

$$\mathbf{P} = \int_{\Omega} \boldsymbol{\mu}(\mathbf{r}) d\mathbf{r}$$

This result is exactly the same as the one obtained for a charge distribution $\rho(\mathbf{r})$ with the total dipole defined by

$$\mathbf{P} = \int_{\Omega} \mathbf{r} \rho(\mathbf{r}) d\mathbf{r}$$

A.3. The quadrupole moment : Q_{2m} .

The same derivation gives for the spherical components of the quadrupole

$$\begin{cases} Q_{22} = \frac{1}{2} \sqrt{\frac{15}{2\pi}} \left[\int_{\Omega} x\mu_x d\mathbf{r} - \int_{\Omega} y\mu_y d\mathbf{r} + i \int_{\Omega} (y\mu_x + x\mu_y) d\mathbf{r} \right] \\ Q_{21} = -\sqrt{\frac{15}{8\pi}} \left[\int_{\Omega} (x\mu_z + z\mu_x) d\mathbf{r} + i \int_{\Omega} (y\mu_z + z\mu_y) d\mathbf{r} \right] \\ Q_{20} = \sqrt{\frac{5}{4\pi}} \left[2 \int_{\Omega} z\mu_z d\mathbf{r} - \int_{\Omega} x\mu_x d\mathbf{r} - \int_{\Omega} y\mu_y d\mathbf{r} \right] \end{cases} \quad (\text{A9})$$

The relations between spherical and cartesian components are given by [53],

$$\begin{cases} Q_{22} = \sqrt{\frac{5}{24\pi}} (q_{xx} - q_{yy} + 2iq_{xy}) \\ Q_{21} = -\sqrt{\frac{5}{6\pi}} (q_{xz} + iq_{yz}) \\ Q_{20} = \sqrt{\frac{5}{4\pi}} q_{zz} \end{cases} \quad (\text{A10})$$

and the traceless quadrupole moment tensor in cartesian coordinates can be written as

$$q_{\alpha\beta} = \int_{\Omega} \left(\frac{3}{2}(r_{\alpha}\mu_{\beta} + r_{\beta}\mu_{\alpha}) - (\mathbf{r} \cdot \boldsymbol{\mu})\delta_{\alpha\beta} \right) d\mathbf{r} \quad (\text{A11})$$

A.4. The octopole moment : Q_{3m} .

The spherical components of the octopole moment may also be computed from Eq.(A4) ; after some algebra, we found

$$\left\{ \begin{array}{l} Q_{33} = -\frac{3}{4}\sqrt{\frac{35}{4\pi}} \int_{\Omega} (\mu_x + i\mu_y)(x + iy)^2 d\mathbf{r} \\ Q_{32} = \frac{1}{2}\sqrt{\frac{105}{8\pi}} \left[\int_{\Omega} \mu_z(x + iy)^2 d\mathbf{r} + 2 \int_{\Omega} (\mu_x + i\mu_y)z(x + iy) d\mathbf{r} \right] \\ Q_{31} = -\frac{1}{8}\sqrt{\frac{21}{4\pi}} \left[8 \int_{\Omega} \mu_z z(x + iy) d\mathbf{r} + \int_{\Omega} (\mu_x - i\mu_y)(x - iy)^2 d\mathbf{r} \right. \\ \quad \left. + 4 \int_{\Omega} (\mu_x(z^2 - x^2) + i\mu_y(z^2 - y^2)) d\mathbf{r} \right] \\ Q_{30} = \frac{3}{2}\sqrt{\frac{7}{4\pi}} \left[\int_{\Omega} \mu_z(2z^2 - x^2 - y^2) d\mathbf{r} - 2 \int_{\Omega} z(\mu_x x + \mu_y y) d\mathbf{r} \right] \end{array} \right. \quad (\text{A12})$$

and the cartesian components of the octopole moment are given by

$$\begin{aligned} \Omega_{\alpha\beta\gamma} = \frac{1}{2} \int_{\Omega} d\mathbf{r} \left[\frac{5}{3}(\mu_{\alpha}r_{\beta}r_{\gamma} + r_{\alpha}\mu_{\beta}r_{\gamma} + r_{\alpha}r_{\beta}\mu_{\gamma}) \right. \\ \left. - r^2(\mu_{\alpha}\delta_{\beta\gamma} + \mu_{\beta}\delta_{\alpha\gamma} + \mu_{\gamma}\delta_{\beta\alpha}) \right. \\ \left. - 2(\mathbf{r} \cdot \boldsymbol{\mu})(r_{\alpha}\delta_{\beta\gamma} + r_{\beta}\delta_{\alpha\gamma} + r_{\gamma}\delta_{\beta\alpha}) \right] \end{aligned} \quad (\text{A13})$$